Published in final edited form as:
Surf Sci. 2015 July 2; 643: 124–137. doi:10.1016/j.susc.2015.06.022.

Initial stages of organic film growth characterized by thermal desorption spectroscopy

Adolf Winkler
Institute of Solid State Physics, Graz University of Technology, Petersgasse 16, A-8010 Graz, Austria

Abstract

In the wake of the increasing importance of organic electronics, a more in-depth understanding of the early stages of organic film growth is indispensable. In this review a survey of several rod-like and plate-like organic molecules (p-quaterphenyl, p-sexiphenyl, hexaazatriphenylene-hexacarbonitrile (HATCN), rubicene, indigo) deposited on various application relevant substrates (gold, silver, mica, silicon dioxide) is given. The focus is particularly put on the application of thermal desorption spectroscopy to shed light on the kinetics and energetics of the molecule-substrate interaction. While each adsorption system reveals a manifold of features that are specific for the individual system, one can draw some general statements on the early stages of organic film formation from the available datasets. Among the important issues in this context is the formation of wetting layers and the dewetting as a function of the substrate surface conditions, organic film thickness and temperature.

Keywords

Organic molecules; Thin films; Thermal desorption spectroscopy; Wetting

1. Introduction

Organic thin films have attracted considerable interest in the recent years. One of the driving forces for this interest is the promising application of organic electronics. In fact enormous progress has been made in the development of organic electronic devices, e.g. for displays, sensors, and solar cells [1-3]. While for many applications polymeric films, fabricated by solution-processing, are used [4], crystalline organic films prepared by molecular beam deposition become increasingly attractive. There exist a number of review articles covering the many aspects of organic thin film preparation [5,6], characterization [7] and application[8-10]. In this article I will focus on the kinetics and energetics of the early stages of organic film formation. I will demonstrate that thermal desorption spectroscopy (TDS) is a very simple, but powerful experimental technique to get insightful information in this context. Questions as to the thermal stability, sticking coefficient, molecule decomposition, wetting layers, dewetting processes, etc. will be addressed. In order to get a more comprehensive understanding we have applied additional experimental techniques, namely in-situ X-ray photoelectron spectroscopy (XPS), low energy electron diffraction (LEED) and work function measurements, as well as ex-situ atomic force microscopy (AFM) and X-ray diffraction (XRD). I will, exemplary, discuss in this review article the adsorption, desorption

Europe PMC Funders Author Manuscripts

Europe PMC Funders Author Manuscripts

and film formation of rod-like organic molecules (quaterphenyl, sexiphenyl) as well as of plate-like molecules (HATCN, rubicene, indigo) on application relevant substrates (gold, silver, mica, silicon dioxide).

2. Experimental

Since in this review I will particularly focus on thermal desorption spectroscopy as a powerful analytical method to characterize organic film growth, I will first make some comments on the most relevant experimental details in this context. For TDS we have used two different quadrupole mass spectrometers (QMSs) allowing measurements up to 200 amu, and 500 amu. In some cases we have measured the intact molecule, but in most cases we have tuned the QMS to some particular cracking masses, which typically give a much higher signal intensity. Nevertheless, we have checked in all cases that the different cracking mass signals as obtained by multiplexing showed the same peak shapes. Any inconsistencies in this behavior would hint to some decomposition/reaction on the surface. Since all the investigated molecules are condensable at room temperature, the desorbing particles can only be detected with a QMS in an in-line configuration. Since for condensable gases the pumping speed is practically infinite, the detected signal is perfectly proportional to the desorption flux [11]. A possible influence of unknown angular and energy distributions of the desorbing particles was not taken into account. However, in contrast to associative desorption (as in the case of hydrogen [12]) where existing activation barriers for adsorption might significantly lead to deviations from cosine angular and thermal energy distributions, we believe that for the organic molecules used these influences are of minor importance.

3. p-Quaterphenyl on Au(111)

Para-quaterphenyl ($C_{24}H_{18}$, m = 306 amu, density ρ = 1.25 g/cm^3) is a rod-like molecule with a Van der Waals length of 2.0 nm (see insert in Fig. 1). Quaterphenyl (4P) is an ideal candidate to study the essential growth features of oligo-phenylenes on application relevant substrates like gold, which is frequently used as contact material in organic electronics. It turns out that clean gold surfaces are rather reactive compared to the commonly used silicon dioxide, which often serves as dielectric gate material. Quantitative TDS reveals that 4P first forms a strongly bound monolayer of flat lying molecules (wetting layer) on Au(111), above which a less strongly bound multilayer develops [13]. This is shown in Fig. 1.

It can immediately be seen that two distinct peaks ($ß_1$, $ß_2$) saturate before the multilayer peak develops, which does not saturate with increasing coverage. The saturation coverage of the $ß_1$ peak corresponds to 0.15 nm and that of the ($ß_1$ + $ß_2$) peaks to 0. 28 nm mean thickness, as determined for the deposited material by a quartz microbalance. Since the Van der Waals thickness of oligo-phenylenes is about 0. 35 nm [14], this is a strong indication that the 4P molecules in the monolayer are lying flat on the surface. The peak shift of the desorption peaks $ß_1$ and $ß_2$ to lower temperature with increasing coverage hints at repulsive interactions between the adsorbed molecules. This is corroborated by LEED investigations. For the $ß_1$ state a well pronounced LEED pattern can be observed which allows a calculation of the oblique surface unit cell of the 4P overlayer with the vector lengths a = 1.44 nm, b = 2.38 nm and a cell vector angle γ of 63° [13]. Comparing this with the Van der Waals

dimensions of the 4P molecules with 2.04 nm length and 0.67 nm width shows that a regular layer is formed in which the molecules are much further apart than the Van der Waals dimensions would allow. The reason for this is that the adsorbed molecules possess a dipole normal to the substrate due to some charge displacement, which results in repulsive forces between the adsorbed molecules. With further increasing coverage the molecules squeeze between the already adsorbed molecules, but due to limited space the molecules become side tilted. Again a well pronounced LEED pattern is observed after saturation of the ß$_2$ peak with a unit cell of a = 1.1 nm, b = 2.2 nm and $\gamma = 74°$ (Fig. 2) [15]. Apparently, the unit cell of the full monolayer, which now contains two molecules, is smaller than that of the semi-layer, due to the attractive quadrupole forces between the flat and side tilted molecules. This epitaxial monolayer acts as a prestage for further film growth, resulting in elongated crystalline islands with the 4P(211) plane being parallel to the Au(111) plane. The side tilting of the molecule in the second semi-layer was additionally verified by NEXAFS investigations [16].

Thermal desorption spectroscopy should in principle allow the determination of desorption energies and frequency factors for the individual monolayer states, based on the Polanyi–Wigner equation (Eq. (1)) [11], as described in detail in many review articles, e.g. by Dietrich Menzel [17], Dave King [18] and many others:

$$R_{\mathrm{des}} = -\frac{dN}{dt} = -\frac{dN}{dT}\beta = \nu \cdot N^{\chi} \cdot \exp\left(-E_{\mathrm{des}}\left(\Theta\right)/kT\right) \quad (1)$$

Here is R_{des}: desorption rate, β: heating rate, ν: frequency factor, N: number of molecules per square unit, x: desorption order, E_{des}:desorption energy, Θ: coverage, T: surface temperature, k: Boltzmann's constant. However, for large organic molecules with many degrees of freedom in the adsorbed state and with lateral interactions between the adsorbed molecules this is not a trivial task [19]. Nevertheless, we have tried to apply the so called "complete evaluation method" proposed by King [18] to the limited number of TD spectra in Fig. 1. We get a desorption energy of 1.3 ± 0.1 eV at small coverage, decreasing to 0.6 eV ± 0.1 eV at 1 monolayer. For the multilayer state (α-peak), which shows a clear zero-order desorption behavior (common leading edge, Fig. 3), quantitative TDS enables calculation of both the desorption energy E_{des} and frequency factor ν independently. In this case in a semi-logarithmic plot of the desorption rate R_{des} versus the reciprocal temperature T the slope of the straight line yields E_{des} and the intercept with the ordinate yields the logarithmic of the pre-exponential factor $\nu \cdot N_0$, with N_0 being the (constant) surface density of the multilayer film. From Fig. 3 we obtain a desorption energy (heat of evaporation) of 1.52 eV/molecule and a pre-exponential factor of $1.23 \cdot 10^{35}$ cm^{-2} s^{-1}. The surface density of the 4P(211) plane of the multilayer has been determined to be $7.7 \cdot 10^{13}$ cm^{-2}, based on XRD measurements [20], which in turn results in a frequency factor of $1.6 \cdot 10^{21}$ s^{-1}.

In a simple picture, the frequency factor ν can be correlated with the attempt frequency of the adsorbed particles to overcome the adsorption potential. In general, and in particular for molecules with a large number of atoms, this perception is not appropriate. The frequency factor actually takes the change of all translational and internal degrees of freedom during

desorption into account. As a result of transition state theory (TST) considerations [17,21] the pre-exponential factor can be described as:

$$\nu = \left(\frac{kT}{h}\right)\frac{q_{\oplus}}{q} \quad (2)$$

with h: Planck's constant, q: partition function of the adsorbed state, $q_{\oplus}$: partition function of the transition state (without the loose vibrational mode normal to the surface which leads to desorption). In the case of non-activated adsorption, the transition state corresponds to the state of the free molecule [22].

For atoms and small molecules the partition functions of the adsorbed and transition state are similar and therefore $\nu \approx kT/h \approx 10^{13}\ s^{-1}$, as frequently observed for typical desorption temperatures between 300 K and 500 K. For large molecules, however, the partition function of the free molecules is, due to the many rotational and vibrational degrees of freedom, much larger than for the adsorbed molecule, where only frustrated rotations and vibrations exist. Therefore, ν is in this case typically many orders of magnitude larger than $10^{13}\ s^{-1}$ [23,24]. Actually, even for the small molecule CO desorbing from metal surfaces "unusually" large frequency factors were described in the literature (e.g. CO/Ru(001) [25], CO/Ni(111) [26]).

4. p-Sexiphenyl on Au(111)

Para-sexiphenyl ($C_{36}H_{26}$, m = 458 amu, density $\rho = 1.29\ g/cm^3$), a rod-like organic molecule with a Van der Waals length of 2.9 nm, shows similarities to the adsorption and desorption kinetics of quaterphenyl, but also exhibits significant differences. These differences can be attributed to the increased number of carbon atoms in the molecule, resulting in a stronger bonding to the substrate (increased desorption temperature) and consequently in a decreased surface mobility, an increased cracking probability on the surface and the formation of a second monolayer. Some of these new features can be seen in Fig. 4, displaying a set of desorption spectra for sexiphenyl (6P) on Au(111) up to a mean thickness of 0.45 nm [27]. Again, we observe two half-monolayer peaks, denoted $ß_1$ and $ß_2$, which again show a peak shift to lower temperature with increasing coverage, indicative of repulsive interactions between the adsorbed molecules. Reasoning behind that is equivalent to that as described for the 4P molecules. LEED experiments have also shown that the $ß_1$ and $ß_2$ peaks are correlated with flat lying and side tilted molecules, respectively. With further coverage increase a new sharp desorption peak appears (denoted $ß_3$), which could be interpreted as a beginning of the multilayer peak. However, further increase of the coverage reveals that this peak again saturates and a new desorption peak at even lower temperature starts to grow, which does not saturate (α-peak), as shown in Fig. 5.

The $ß_3$ peak saturates at about 0.7 nm, which corresponds roughly to two layers of flat lying 6P molecules. Thus, we can draw the conclusion that a second layer of flat lying molecules adsorbs on top of the first, more strongly bonded monolayer, above which elongated multilayer islands grow, as shown by AFM measurements [28]. The $ß_3$-peak is very narrow and resembles a zero-order desorption characteristic. A possible explanation for such desorption behavior could be the coexistence of 2D islands in the second layer being in

equilibrium with a 2D gas phase, where desorption is equally possible from both states, as suggested by Opila and Gomer [29]. This interpretation is further supported by the fact, that the second 6P layer produces only a single peak compared to the two distinctive peaks in the first monolayer.

From the multilayer peak, which again shows a common leading edge, we have calculated the desorption energy E_{des} = 2.4 eV and the frequency factor $\nu = 5.6 \cdot 10^{25}$ s^{-1}. For this analysis a constant surface coverage of $5.4 \cdot 10^{13}$ molecules/cm^2 was used, which was calculated from the molecule density in the 6P(21-3) plane, that lies parallel to the substrate surface, as determined by XRD measurements on a 30 nm thick 6P film on Au(111) [30]. If we compare the desorption energies for multilayer desorption (heat of evaporation) (1.52 eV for 4P and 2.4 eV for 6P) we see a nearly perfect linear relationship between the heat of evaporation and the number of carbon atoms in the individual molecules, resulting in a share of about 65 meV per C-atom. One can speculate that a similar relationship should exist for the single nP molecules adsorbed on the Au(111) plane. For this discussion we compare the desorption peak temperatures by extrapolating the ß$_1$ peaks in Figs. 1 and 4, respectively, to zero coverage yielding $T_p \approx 560$ K for 4P and $T_p \approx 680$ K for 6P. One could use the Redhead equation for first-order desorption, which relates the peak maximum to the desorption energy [11]: E_{des} [cal/mol] $\approx (\ln(\nu \cdot T_p) - 3.64) \cdot RT_p$, with R = 2 cal/(mol·K), for heating rate 1 K/s. Unfortunately, using this equation requires the knowledge of the frequency factors, which are not known in our case. However, one can make an estimate of the necessary ratio of ν(6P)/ν(4P) in order to fulfill the assumption that the contribution of a single C-atom to the binding is the same for 6P and 4P. It turns out that this ratio is approximately 10^4. Interestingly, the ratio of the frequency factors for multilayer desorption ($5.6 \cdot 10^{25}$ s^{-1} for 6P, $1.6 \cdot 10^{21}$ s^{-1} for 4P) is of the same order. Which information can we get from these results? As mentioned above, the frequency factor is related to the ratio of the partition functions in the free state and the adsorbed state. The lower the partition function in the adsorbed state (i.e. the less mobile the molecules are) the larger is the frequency factor. The above result indicates that the 6P molecules at low coverage are much less mobile on the Au(111) plane than the 4P molecules, which is exactly what we have expected for the larger molecule, because more C-atoms contribute to the (Van der Waals) bonding.

Next we will address another feature of 6P adsorption which is closely related to the stronger bonding for the larger molecule. A closer inspection of Fig. 4 shows immediately that the desorption trace after deposition of 0.16 nm mean thickness is much smaller than expected, indicating that some adsorbed material does not desorb during sample heating. In Fig. 6 we have plotted the amount of desorbed material versus the exposed amount for 6P on Au(111), as determined by a quartz microbalance, together with the results for some other systems. It shows that, at least for higher coverages, about 0.2 nm mean thickness of 6P (about ½ monolayer, i.e. the flat lying molecules) does not desorb during heating. This compilation also shows impressively the influence of molecule size and substrate material on the decomposition of nP molecules. While the decomposition for 6P on the Au(111) surface is considerable, nearly no decomposition takes place for the smaller 4P molecule. On the other hand 4P on a stepped gold surface Au(433) and also on a polycrystalline gold foil shows already some decomposition of about 0.1 nm mean thickness. Moreover, 6P on a

polycrystalline gold foil decomposes severely. The amount of 0.3 nm indicates that practically the full first layer, composed of flat lying and side tilted molecules, decomposes during heating.

In the following we address the question at which substrate temperature this decomposition takes place and of which type the remaining species are. For this purpose we have tuned our mass spectrometer not only to a single cracking mass of 6P (typically mass 61 amu) but also to other possible cracking products, in particular hydrogen. In Fig. 7 we can clearly see that after deposition of 0.2 nm of 6P on a sputter cleaned Au(111) substrate (trace #1) not only 6P desorbs but also a certain amount of hydrogen. The desorption of hydrogen starts immediately after 6P desorption and at least two hydrogen desorption peaks can be observed. A subsequent Auger analysis clearly shows carbon contamination on the gold substrate. If we deposit again 0.2 nm 6P on this partially carbon covered Au surface significantly more 6P desorbs and the amount of desorbing hydrogen decreases. After several adsorption/desorption cycles a carbon saturation layer is formed on which no further 6P decomposition can take place.

The existence of at least two hydrogen desorption peaks suggests that 6P decomposition does not take place in form of a single process. One has rather to assume that, in addition to a partial first dehydrogenation process, some more stable polycyclic aromatic hydrocarbons (PAHs) are produced, e.g. by cyclo-dimerization, which then finally decompose at higher temperature [31]. A proposed scenario for such a dehydrogenation/cyclo-dimerization is shown in Fig. 8 for quaterphenyl, which showed similar cracking features as for sexiphenyl [32]. We could indeed demonstrate by LEED that after heating the sample to a temperature above the first hydrogen desorption peak a 6-fold diffraction pattern was observable, which fitted quite well to a regular structure of such PAHs. However, the very broad diffraction spots indicated that the regular domains composed of the PAHs are quite small (3–4 nm in diameter) [27].

5. p-sexiphenyl on mica (001)

Mica is a frequently used substrate for investigating adsorption and initial film growth of organic molecules. The reason behind that is that one can easily prepare well-defined single crystal surfaces by just cleaving mica foils and immediately install those “freshly cleaved” samples into a vacuum chamber. Contrary to metal surfaces, which would of course immediately contaminate in air, mica surfaces remain more or less unchanged for some time after the cleaving procedure. Another advantage of mica is that one can significantly change the adsorption and growth behavior by modifying the surface either via carbon contamination or via sputtering. The deposition of 6P on freshly cleaved mica yields very long needle-like islands [33,34]. Such nanostructures are suggested to be applicable for nano-optic devices [35]. One of the questions as discussed at that time was related to a possible wetting layer in between the needle-like islands. In Fig. 9a a series of TD spectra is depicted for different coverages up to 0.6 nm mean thickness, while an AFM image of a 1 nm thick film is shown in Fig. 9b [36].

One can clearly see the development and saturation of a monolayer peak (ß) followed by a multilayer peak (α) at higher coverages. There is only a single monolayer peak present with a saturation of around 0.2 nm. Unfortunately, no reliable LEED investigations of the 6P monolayer on mica(001) exist. Additionally, the crystallographic orientation of the multilayer needles was examined by XRD [37]. It was found that the 6P(11-1) and 6P(11-2) crystallographic planes are aligned parallel to the mica(001) substrate for certain film preparation temperatures. In both cases the 6P molecules within those planes are nearly parallel to the mica surface. Furthermore, the needles are azimuthal aligned due to epitaxial ordering. The needle direction is close to the [110] direction of the mica (001) surface.

The reason for the flat lying molecules in the monolayer and the alignment of the needle like islands, in which the molecules are again oriented nearly parallel to the substrate, can be found in the very specific nature of the mica (001) surface. Mica is a silicate mineral ($KAl_2(AlSi_3O_{10})(OH)_2$), consisting of consecutive layers of K, Al, SiO_4 and OH, which cleaves along the basal plane by exposing half a monolayer of K atoms. The K atoms are positively charged and this charge is balanced by a negative charge in a deeper layer, where some of the positively charged Si^{4+} are substituted by Al^{3+} ions. This leads to a dipole field with a component parallel to the surface [38]. It is postulated that this is the main reason for the strong alignment of elongated organic molecules on mica(001) [39]. If this is indeed the case, then a destruction of this dipole field by a change of either the surface chemistry or the surface structure, should severely influence the layer growth of 6P. This was observed indeed and will be described in the following.

A freshly cleaved mica surface, even after being installed immediately into the UHV chamber, is not perfectly clean. XPS shows carbon contamination which we have estimated to be about ½ monolayer. Nevertheless, on such a surface a clear 6P wetting is observed and needle-like island formation takes place. However, when we increase the carbon coverage beyond this initial value the wetting layer fades away. This is shown in Fig. 10a for various C-coverages between ½ and 1 monolayer. The increased C contamination was produced by depositing a thick layer of 6P (>10 nm) at 100 K onto the mica surface and subsequently exposing it to the MgK_α radiation of an X-ray gun. A TD-flash was used to get rid of the remaining 6P, but additional carbon accumulation was observed on the surface. With this method we could increase the C content up to 1 monolayer, for which no 6P wetting layer could be seen anymore. The AFM image of such a 6P film shows a dramatic change of film morphology (Fig. 10b). Instead of needle-like islands, more or less circular islands have developed with a height of roughly 2.7 nm. This is a clear indication of islands composed of standing 6P molecules. In most cases already a second layer started to form on the first layer, which is likewise composed of standing molecules. Apparently, no wetting layer exists between the islands.

A very similar result is obtained when destroying the regular arrangement of the surface atoms by gentle sputtering with Ar^+ ions. Typically, we used a beam energy of 500 eV. With the help of Auger electron spectroscopy we were not able to observe significant changes of the surface composition, thus we conclude that the changes in 6P film formation, caused by sputtering, are rather a result of structural changes of the surface. This was supported by LEED investigations, which showed the disappearance of the regular LEED pattern upon

sputtering. The influence of sputtering on the wetting layer is demonstrated in Fig. 11a, while the corresponding morphology of the 6P film is shown inFig. 11b. The influence of sputtering on the wetting layer is similar to that of carbon contamination. However, there is a slight difference in the film morphology, as shown in the AFM image (Fig. 11b). For that case the formation of a second layer is not yet observed, although the total coverage (1 nm) is the same as in Fig. 10b. This hints at a decreased Ehrlich–Schwöbel barrier [40,41] for step-down diffusion of the 6P monomers on the first layer. However, the processes behind this difference are not clear until now.

6. HATCN on Au(111)

So far we have focused on the initial film growth of rod-like organic molecules on solid substrates. Another type of organic molecules, which also exhibit promising features for the application in organic electronics, are of plate-like character. We have focused on the growth behavior of the discoid molecule hexaazatriphenylene–hexacarbonitrile (HATCN, $C_{18}N_{12}$, m = 384 amu, density $\rho = 1.6$ g/cm^3, Van der Waals diameter: 1.5 nm) on metal surfaces. It has been proposed that these molecules could be used as buffer layers between metal contacts and organic semiconductors in organic devices [42]. Indeed, these molecules show a very intriguing adsorption/desorption behavior, which can be best characterized by TDS [43]. Fig. 12 shows a series of desorption spectra for HATCN on Au(111), deposited at 200 K.

At coverages below one monolayer the desorption behavior is similar to that of 6P on Au(111). We observe two desorption peaks, denoted $ß_1$ and $ß_2$, both shifting to lower temperature with increasing coverage, due to repulsive dipole interaction. The saturation of these peaks at approximately 0.15 nm and 0.3 nm, respectively, demonstrates that the molecules are again lying flat on the surface. With further coverage increase, a new peak (denoted γ-peak) appears at lower temperature, which saturates at about 0.6 nm. This peak is a clear indication of a second layer of flat lying molecules. However, this adsorption state is metastable, since with further coverage increase the γ-peak starts to decrease and a new peak at higher temperature develops. This peak (denoted α) does not show saturation with further coverage increase and can therefore be correlated with desorption from a multilayer. The interesting feature is the full dewetting of the second layer, whereas the first layer is not involved at this stage. Actually, such rather unusual desorption behavior has been observed already quite early for benzene on Ru(001) by Polta and Thiel [44] and later by Jakob and Menzel [45], who have discussed this phenomenon in detail. The reason for the phase transition is most likely the increased interface energy between the 2nd and 3rd layer. According to Szalay et al. [46] the HATCN molecules avoid π-π stacking. The crystal packing of HATCN is instead dominated by perpendicular CN-π interactions (T-stacking). Therefore, small amounts of molecules in the 3rd layer act as nucleation centers for the formation of three-dimensional islands. The binding energy of the molecules in the first layer is apparently strong enough that these molecules do not contribute to dewetting.

However, a quite intriguing feature is observed when the coverage is further increased (Fig. 13). While the multilayer α-peak increases, desorption from the $ß_1$ and $ß_2$ monolayer peaks starts to decrease. We could demonstrate by ex-situ AFM experiments that the decrease of

monolayer desorption roughly correlates with the surface area covered by multilayer islands [43]. Thus, we conclude that the molecules in the first layer, when covered by islands, rearrange to the bulk structure, from where they then desorb already at lower temperature compared to that of the uncovered monolayer. Such an incorporation of molecules, which are stable in the monolayer at high temperature, into a 3D phase that desorbs at lower temperature has, to the best of our knowledge, not been reported before.

The question now arises at which temperature the dewetting process takes place. For this purpose, we have performed XPS measurements, where we followed the change of the Au4f core level signal as a function of coverage and temperature. This is a suitable method to investigate morphological changes in a film, e.g. a transition from a layer-like film to an island-like film. In Fig. 14 the $Au4f_{7/2}$ intensity vs. temperature is compiled for various initial HATCN coverages, after film formation at 200 K. For initial coverages up to 0.3 nm the Au4f signal does not change up to 500 K above which the signal increases due to desorption of the ß-states. For the 0.5 nm film (trace d) the sharp signal increase at 450 K corresponds to desorption from the γ-state. For higher initial coverages (trace f–h) the XPS signal shows a first sharp increase already at about 350 K where no desorption takes place. This is a clear indication of a morphological transition from a layer-like film to a 3D island-like film. We could prove this growth behavior also by AFM, where 2 nm thick HATCN films on Au(111), grown at 300 K, show a continuous film, while comparable films grown at 400 K show a strong island-like film morphology [43].

The evaluation of desorption energy and frequency factor for the multilayer has been done as described before and yields $E_{\mathrm{des}} = 1.84 \pm 0.1$ eV and $1 \times 10^{19\pm 1}\ \mathrm{s}^{-1}$, respectively. For this system, we have tried to determine these values also for the $ß_1$ and γ peak, which both exhibit a clearly defined peak maximum for saturation of the individual states. In this case, we have applied the evaluation method proposed by Redhead, using the heating rate dependence of the desorption peak maximum. For a first-order desorption process the following relationship holds [11]:

$$\frac{E_{des}}{RT_m^2} = \frac{\nu}{ß}\exp\left(\frac{-E_{des}}{RT_m}\right) \quad (3)$$

Here, ß is the heating rate and T_m the peak maximum. Therefore, a plot of $\ln(ß/T\,2m)$ vs. $1/T_m$ should result in a straight line where the slope yields the desorption energy and the intercept with the y-axis yields the pre-exponential factor. From a set of spectra for heating rates between 0.3 K/s and 3 K/s we obtained the following values: $ß_1$-state: $E_{\mathrm{des}} = 1.7 \pm 0.2$ eV, $\nu = 1 \cdot 10^{12\pm 2}\ \mathrm{s}^{-1}$; γ-state: $E_{\mathrm{des}} = 2.0 \pm 0.2$ eV, $\nu = 1 \times 10^{21\pm 2}\ \mathrm{s}^{-1}$. The error for this type of evaluation is by nature larger than for a leading edge evaluation of zero-order desorption, due to the limited range of the heating rate variation. Nevertheless, the result of this evaluation is very intriguing. The desorption energies for all three adsorption states (α, β_1, γ) are nearly the same (within error). Actually, there is even an opposite trend between the desorption peak maxima and the desorption energies. Hence, the difference of the desorption temperatures for the individual adsorption states is mainly determined by the pre-exponential factors. Both the multilayer peak (α) as well as the second layer peak (γ) exhibit the large pre-exponential factor expected for large molecules. Surprisingly, the monolayer

peak (β_1) shows a very small pre-exponential factor, usually only observed for small particle desorption (atoms, diatomic molecules). The following conclusion can be drawn from this result: At the desorption temperature the partition function of the molecules in the first monolayer is similar to that in the gaseous phase. In other words, the translational and rotational degrees of freedom are already highly excited in the adsorbed phase when desorption starts. Apparently, the activation energy for surface diffusion of the large HATCN molecules on the inert gold surface is very small and the molecules behave like a two-dimensional gas. The high pre-exponential factors for desorption from the second layer and the bulk phase indicate that only little excitation of the various degrees of freedom takes place prior to desorption (with the exception of the translation normal to the surface). This is the case if the molecules are rather immobile prior to desorption.

7. HATCN on Ag(111)

The adsorption/desorption behavior of HATCN on Ag(111) shows some remarkable differences compared to that on the Au(111) surface. Up to a mean thickness of 0.24 nm no desorption of HATCN can be observed at all. However, there is clear evidence that HATCN is adsorbed on the surface. LEED experiments reveal a clear (7 × 7) superstructure at a coverage of 0.24 nm [47]. This coincides perfectly with STM measurements, which demonstrated that HATCN forms a regular honeycomb structure at this coverage, which is characterized by a hexagonal unit cell with a lattice parameter of 2.0 nm, containing two molecules in the unit cell [42]. When heating such a film up to 900 K no desorption of HATCN or other fragments takes place. However, the regular LEED pattern disappeared upon heating and did not reappear after cooling to room temperature. It was speculated that during heating a polymerization of the adsorbed and fragmented molecules takes place by forming paracyanogen, which is stable up to 1100 K [47].

For coverages between 0.24 nm and 0.8 nm mean thickness still no desorption of intact HATCN can be seen. However, in this intermediate regime desorption of particles with mass m = 52 amu is observed between 600 K and 900 K (see Fig. 15). This mass can be attributed to C_2N_2. We could verify that this QMS signal is not the cracking mass of molecules with higher mass. That means that C_2N_2 stems directly from fragmentation on the surface. This signal saturates at about 0.8 nm mean thickness.

The question as to the nature of the adsorbed HATCN layer up to and at 0.8 nm mean thickness now arises. This thickness corresponds to an areal density of $2 \cdot 10^{14}$ molecules/cm^2, or about 3.5 monolayers of face-on oriented molecules. However, such a configuration can be ruled out, because in this case at least some of the molecules should be physisorbed and therefore desorb already in intact form. Additional experimental investigations using XPS, infra-red spectroscopy and work function measurements suggested that the molecules above one monolayer start to change from a face-on configuration to an edge-on configuration with increasing coverage, already at 200 K. This reorientation was furthermore confirmed by DFT calculations [48]. Such a layer does not favor polymerization into a stable paracyanogen layer up to the highest applied temperature, instead detachment of fragments can be possible. Those CN groups pointing away from the surface separate from the molecule and desorb associatively as C_2N_2. The reason for the

appearance of two distinct peaks in Fig. 15 is not yet clear. However, associative cyanogen desorption from Pt(110) also features two desorption peaks in the same temperature range [49]. Unfortunately, an explanation for this behavior was not given.

Above a HATCN mean thickness of 0.8 nm, where desorption of cyanogen becomes saturated, desorption of intact HATCN molecules starts to appear. The corresponding desorption spectra are shown in Fig. 16a for low coverages and in Fig. 16b for higher coverages.

In Fig. 16a the development of two peaks, designated γ and α′, with an intensity ratio of about 2:1, can be observed. These two peaks saturate roughly at a total coverage of 1.36 nm. Based on the coverage of this layer, corresponding to 0.48 nm, and the 2:1 ratio of the two peaks, we propose that this layer is composed of more strongly bonded face-on oriented molecules (α′-peak) and of less strongly bonded edge-on oriented molecule (γ-peak), on top of the first layer, which is composed of standing molecules. Such an arrangement of HATCN molecules is indeed very likely, because the bulk structure is based on T-stacking [46]. The fact that the 2:1 ratio between γ and α′ is nearly constant throughout the development of this layer implies that this layer grows in form of islands.

However, this second layer is metastable. Just a little additional material that evaporated onto this layer leads to a rapid destabilization and dewetting. This is shown in Fig. 16b, where both desorption peaks (γ and α′) start to decrease and a new peak, denoted α, increases. This decrease cannot be seen so nicely for the α′ peak when compared to the γ peak, but a closer inspection of the trailing edge reveals that there is not a simple shift of the α′ peak into the α peak. The latter peak, which does not show saturation, represents of course desorption from multilayer islands. Thus, in this coverage regime a similar dewetting behavior takes place as for HATCN on Au(111). Just a little amount of HATCN in the third layer leads to an energetically unfavorable interface, driving the dewetting process. Similar temperature controlled XPS measurements as performed for the HATCN-Au(111) system revealed an almost identical dewetting temperature of about 350 K [47].

Finally, we have performed calculations of the desorption energy and frequency factor for the multilayer α-peak. Using a desorption spectrum of a 6 nm thick film (not shown) we calculated a desorption energy of 1.9 ± 0.1 eV and a frequency factor of $8 \cdot 10^{18\pm 1}\ s^{-1}$. For this calculation we have taken a surface density of $1.8 \cdot 10^{14}$ HATCN molecules/cm^2, based on the molecule mass of 384 amu and a bulk density of 1.6 g/cm^3 [46]. This result is in good agreement with the values obtained for HATCN multilayer desorption from Au(111), as one would expect.

8. Rubicene on SiO_2

So far, we have mainly focused on the adsorption and desorption behavior of organic molecules on metal substrates, which can be used as contact material in organic electronic devices. In addition, dielectric substrates have to be applied as well, e.g. as gate material in organic transistors. Although it is desirable to use organic dielectrics too, silicon dioxide is still a frequently used material as gate dielectric for organic model transistors. In this paragraph, we report on the adsorption and initial film formation of rubicene on SiO_2.

Rubicene (C_{26},H_{14}, m = 326 amu, ρ = 1.39 g/cm^3) is a polycyclic hydrocarbon consisting of five benzene rings with three linearly fused rings and one benzene ring at each diagonal side, shown in the inset of Fig. 17. This plate-like organic molecule again shows some quite intriguing adsorption and desorption features. First, some comments to the silicon dioxide substrate. The 150 nm thick thermally grown oxide on a 0.6 mm thick Si(100) wafer has a quite poorly defined surface structure and stoichiometry. In addition to hydroxyl groups on the surface, carbon is typically observed as contaminant. The carbon can be easily removed by sputtering; however, repeated heating of the sample results in further carbon segregation. Similarly, repeated adsorption/desorption cycles led to carbon contamination as well. Interestingly, the carbon contamination had only some quantitative influence on the adsorption behavior; qualitatively it was the same on a C-contaminated and a sputter-cleaned surface [50]. Therefore, we will only focus on the interaction of rubicene with sputter-cleaned silicon dioxide.

Fig. 17 shows a set of thermal desorption spectra of rubicene from clean silicon dioxide, deposited at 220 K and heated with a rate of 1 K/s. The exposure is given in Hz; according to the calibration with a quartz microbalance 1 Hz is equal to a mean thickness of 0.09 nm, if the sticking coefficient is assumed to be one. In this context, we have to note that the given temperatures in the TD spectra are not the temperatures of the SiO_2 surface. The silicon wafer is clamped onto a heated stainless-steel plate, on which the temperature is measured (this is necessary for the linear heating regulation). However, one can apply a simple first-order temperature correction (see supplement of Ref. [50]), the corrected temperatures are also shown in Fig. 17. First, it has to be mentioned that dissociation of rubicene on the clean silicon dioxide surface is not significant in a single adsorption/desorption cycle, contrary to most metal substrates. Nevertheless, after each adsorption/desorption cycle the surface was again sputtered. For low exposure (2–17 Hz) a single desorption peak (α) appears at an (uncorrected) temperature of about 540 K. With increasing coverage, the peak shifts to higher temperature with a common leading edge. This particular desorption behavior can either be explained as being due to desorption from a mixed layer of condensed 2-dim. islands and a 2-dim. gas phase [29], as already mentioned for the system 6P on Au(111), or by attractive forces acting in the adsorbed layer. We prefer the latter explanation, in particular because with further coverage increase even a shift of the leading edge to higher temperature is observed (exposure of 20 Hz and 25 Hz). However, this layer is metastable; after a small additional exposure (30 Hz) this desorption state suddenly disappears and a new desorption peak (ß) at around 650 K appears, which increases with further exposure and shows zero order desorption kinetics. Accompanying AFM investigations show that this film is composed of islands [50]. Apparently, for low coverage the rubicene molecules are rather weakly bonded. Increasing the coverage beyond a certain value leads to a sudden dewetting and island formation, in which the molecules are more strongly bonded.

In order to quantitatively determine the coverage at which dewetting sets in one has to calculate the sticking coefficient. For this purpose we plotted the area of the desorption spectra as a function of the exposure, as depicted in Fig. 18. This yielded the interesting result of the sticking coefficient not being equal to one independent of the coverage, as it is frequently assumed and in fact experimentally observed for many systems. The sticking

coefficient, which is proportional to the slope of the curve in Fig. 18, continuously increases with increasing coverage. If we assume that the largest slope at high coverage corresponds to a sticking coefficient of one, then the initial sticking coefficient is just 0.17. A similar small value of $s_0 = 0.25$ was measured for rubicene on the carbon saturated SiO_2 surface. Based on these results, we can estimate the coverage of the α peak in Fig. 17, at which dewetting starts, which turns out to be a layer of about 0.4 nm mean thickness. This again underlines that, after the formation of one monolayer of flat lying molecules, additional molecules cause a destabilization of the layer followed by immediate dewetting and island formation. A similar behavior was observed for rubicene on the carbon covered SiO_2 surface, but the data suggest that in this case dewetting occurs above two layers of flat lying molecules [50].

Coverage and/or temperature induced dewetting of organic thin films seems to be a quite general feature. In addition to that, one has to put up the question if exposing a thin organic film to air also might change the morphology of the film. This can indeed be the case and shall be demonstrated for this system. Exposing a C-covered SiO_2 surface to 7 Hz of rubicene yields a mean thickness of 0.16 nm and the film desorbs nearly exclusively as α-peak, i.e. from the wetting layer, as shown in Fig. 19, curve (a). However, when preforming an ex-situ AFM analysis for this film we see only islands (inset in Fig. 19). Actually, an integration over all islands shows that all material is contained in the islands and there is no hint of a remaining wetting layer. This behavior has to be explained by a dewetting process caused by the exposure of the sample to air. Such a venting induced dewetting has also been demonstrated for the system hexaphenyl on mica [51]. Indeed, after reinstalling the air exposed film into the vacuum chamber and performing a TD experiment after re-evacuation showed a dramatically different desorption spectrum (Fig. 19, curve (b)). Only desorption in form of the ß-peak, i.e. desorption from multilayer islands is observed. In addition, the total area under the desorption spectrum has decreased by about 40% after venting, which is mainly due to desorption during air exposure.

Finally, we have determined the desorption energy and the frequency factor for multilayer desorption. For this purpose, we have adsorbed/desorbed a multilayer of rubicene (9 nm) onto the stainless steel plate, in order to avoid the temperature correction which would be necessary for desorption from the silicon sample. We obtain a desorption energy of 1.47 ± 0.05 eV and a frequency factor of $\nu = 3 \cdot 10^{18}\ s^{-1}$. (See supporting information of Ref. [50]).

9. Indigo on SiO_2

Recently, hydrogen bonded organic material have attracted quite some interest in the community of organic electronics. One important example of such a material is the natural dye indigo. It has been shown that indigo has excellent semiconducting properties and field effect transistors with good performance have been fabricated already [52]. One interesting feature of such type of organic material is that they can be part of “green and biodegradable electronics” [53]. Still, one of the big challenges in this context is the creation of well-defined thin films. Therefore, we have studied the adsorption and desorption behavior of indigo on silicon dioxide surfaces in some detail.

Indigo ($C_{16}H_{10}N_2O_2$, m = 262 amu, density $\rho = 1.50$ g/cm^3) shows very low solubility, due to the strong intermolecular hydrogen bonds, and the preferred method of film formation is physical vapor deposition. In comparison to the adsorption/desorption behavior of rubicene on silicon dioxide some similarities can be observed, in particular the dewetting of a weakly bound monolayer into a more strongly bound multilayer phase. On the other hand there are also peculiar differences. In particular, indigo shows a very different initial growth behavior when adsorbed on clean and carbon covered silicon dioxide. As described before, several adsorption/desorption cycles on a clean substrate lead to a carbon saturated surface which is then stable against further decomposition of indigo [54].

A set of thermal desorption spectra of indigo from carbon covered silicon dioxide in the low coverage regime is shown in Fig. 20. Both the measured and the corrected temperatures are depicted (see supporting information of Ref. [54]). A quartz frequency change of 1 Hz corresponds to an exposed amount of 0.08 nm mean thickness. The evaluation of the adsorbed amount versus the exposed amount reveals that the sticking coefficient is constant over a wide coverage range [54]. Thus, we assume that the sticking coefficient is one for indigo on C-covered silicon dioxide. Up to a coverage of 0.08 nm mean thickness a single peak is observed, denoted as α-peak, at a corrected temperature of 290 K. With further exposure this peak decreases and a new peak, denoted ß-peak, appears at a corrected temperature of about 350 K. Above coverages of about 1 nm the α-peak has totally disappeared and the ß-peak increases with further exposure, showing typical signs of zero-order desorption. Evaluation of the multilayer spectra as usual yields a desorption energy of 1.67 ± 0.05 eV and a frequency factor of $1 \cdot 10^{22}$ s^{-1} [54]. The transformation of the α-peak into the ß-peak is again a clear indication of a coverage dependent dewetting from a weakly bound first layer into a multilayer phase in which the molecules are more strongly bound. The interesting point in this case is that the dewetting process already starts at a coverage of about a ¼ monolayer of flat lying molecules.

The situation is quite different for the adsorption of indigo on a sputter-cleaned substrate. (Again, in this case the surface was sputter-cleaned after each adsorption/desorption cycle.) A set of TDS is shown in Fig. 21. In this case, for coverages of up to 0.16 nm (2 Hz) no indigo desorbs at all. The molecules rather decompose on the surface upon heating. However, with further exposure, the α-peak appears and reaches a maximum at a coverage of about 0.48 nm (6 Hz) before it disappears again and the material desorbs at higher temperature in form of the ß-peak. Although the latter behavior seems to be similar to that as observed for the carbon-covered surface, there exists an intriguing difference. This becomes evident when examining the coverage-exposure relationship in more detail, as shown in the inset of Fig. 21. When increasing the exposure in a quite narrow range above 0.16 nm suddenly the material, which did not desorb at all below this coverage, desorbs nearly completely. Further inspection of the coverage-exposure relationship reveals a linear behavior above 3 Hz (0.24 nm), thus, we can again safely assume that the sticking coefficient is one, independent of the coverage. The extrapolation of this line yields an intercept with the x-axis at about 1 Hz (0.08 nm), indicating the amount of decomposed indigo after each adsorption/desorption cycle. Nevertheless, the strange desorption behavior in the coverage range around 0.2 nm seems to be a puzzle.

Within our current understanding we describe the film formation and desorption behavior on the sputter cleaned surface as follows: Initially, single molecules adsorb on the surface and form chemical bonds that are so strong, that no desorption occurs. One contribution to the strong bonding can be attributed to hydrogen bonds between the flat lying indigo molecules and the substrate (Fig. 22a). As soon as a certain coverage threshold of about 0.2 nm mean thickness is reached, the probability of newly impinging molecules to land on top or in the vicinity of already adsorbed monomers becomes high enough, for a structural re-orientation to take place. We suggest, that dimers are formed, where each indigo molecule establishes hydrogen bonds to another indigo molecule. These dimers are now more weakly bonded to the substrate due to the newly created hydrogen bonds between the active groups in the dimer. Situations where adsorbed molecules rearrange and form dimers with specific H-bonding interactions, thus causing increased diffusion on the surface have indeed been reported in the literature [55,56]. Similarly, the formation of porphyrin dimers on Cu(111) with increased diffusivity has been demonstrated by high resolution STM [57]. With our experimental capabilities we can of course not present any evidence as to the type of the dimer or multimer formation, but we do suggest a parallel π-stacking configuration where one molecule lies on top of another molecule with reversed handedness (Fig. 22b). At a coverage above 0.5 nm mean thickness dewetting sets in and island formation takes place again, similarly to that on the carbon covered silicon oxide surface. The significantly higher saturation coverage of the α-state is due to the dimer formation.

10. Summary and conclusions

The investigation of adsorption, desorption and initial film growth for a variety of organic molecules reveals, on the one hand, a manifold of features which are very specific for the individual systems, but on the other hand allows also for making some very general statements on the interaction of organic molecules with solid surfaces. It is obvious that for a comprehensive characterization of organic film growth (structure, morphology, energetics, kinetics) many analytical tools have to be applied. However, in this article I wanted to emphasize the power of thermal desorption spectroscopy, in particular to elucidate the kinetics and energetics of organic thin film formation. In order to complete and support the gained results, in-situ XPS, LEED and work function measurements, as well as ex-situ AFM and XRD were applied.

Unfortunately, the dream of many users, in particular of the organic electronic community, to be able to fabricate perfect layer-like organic thin films (Franck-Van der Merwe growth) can hardly be fulfilled. Based on the experimental results of this work and also based on other relevant literature data [58-63] one can essentially define two different scenarios for the film growth of elongated and plate-like organic molecules. In the first scenario the substrate is very reactive (e.g. Au, Ag, other clean metal surfaces, freshly cleaved mica) and the organic molecules first adsorb flat on the surface by forming a strongly bound wetting layer, above which the multilayer film grows in the form of islands (Stranski–Krastanov growth). The first layer typically acts as a template for the thicker (multilayer) film, which means that the arrangement of the molecules in this layer already depends on the bulk structure. For example, the rod-like organic molecules p-quaterphenyl and p-sexiphenyl crystallize in the herringbone structure, where in the bulk along a specific net plane flat-on

and side-on molecules are arranged next to each other, layer by layer [64]. Consequently, when these molecules form a saturated wetting layer, this layer is also composed of flat-on and side-on oriented molecules, which exhibit different adsorption energies. Hence, a double peak is observed in the desorption spectrum. For the face-on oriented molecules (1st half monolayer) some charge transfer may take place, which leads to dipoles normal to the surface. Thus, repulsive forces act between nearby adsorbed flat-lying molecules, leading to a shift of the desorption peaks to lower temperatures with increasing coverage. Another consequence of this repulsion is that in the sub-monolayer regime no islanding is observed. With further exposure, additional molecules squeeze in between the flat-on oriented molecules and take a side-on configuration. In this case, (attractive) quadrupole forces can be active leading to a more compact layer. Further molecules impinging on the wetting layer experience a rather unreactive surface. The monomers are very mobile on this wetting layer and dipole repulsion is negligible. Therefore, layer growth will first proceed in form of 2D and subsequently of 3D islands. The molecules will be incorporated in these islands again with their long axes parallel to the surface, either flat-on or side-on, depending on the orientation of the underlying molecules. XRD investigations show that the 3D islands are not only perfect crystals, but also that the crystals are oriented in such a way that the net-planes parallel to the surface are composed of face-on and side-on oriented molecules. In the case of a Au(111) surface these are the 4P(211), 4P(311) [13] and 6P(21-3) planes [30]. In addition, as there exists also azimuthal alignment, the growth of organic molecules on single crystal metal surfaces can typically be described as epitaxial growth. Since the diffusion probabilities of the monomers on the wetting layer depends on the diffusion direction and, furthermore, the incorporation probability of the approaching monomers in the existing islands, which in turn may depend on the relative orientation, the growing islands are typically of elongated shape. A special case is the system 6P on mica(001), where extreme length/width aspect ratios of more than 100 can be observed [36]. In thermal desorption spectroscopy the desorption peak corresponding to the multilayer islands appears at lower temperature than that of the monolayer.

In the second scenario, the surface is quite unreactive with respect to the organic molecules. Examples are carbon covered metal surfaces, silicon dioxide or amorphous mica. On such surfaces, the monomers are again flat-lying, but weakly bound and very mobile. If several diffusing monomers encounter each other, they may form a super-critical cluster by reorientation into an energetically more favorable arrangement and these clusters, composed of standing molecules, will grow by incorporation of further monomers (diffusion-limited aggregation [65,66]). In this case, no stable monolayer exists (Vollmer–Weber growth). With thermal desorption spectroscopy only a single desorption peak is observed, which stems from 2D or 3D islands. Examples are 6P on C-covered mica [36] and 6P on KCl(001) [67]. XRD shows that for the rod-like molecules, which crystallize in a herringbone structure, the corresponding islands are typically composed of crystals with the (001) plane parallel to the substrate surface, i.e. the molecules are oriented nearly normal to the surface. The morphology of the islands resembles aztec pyramids with round or dendritic footprints [68]. Due to this type of film formation, again no layer-by-layer growth on the large scale can be achieved.

Besides these two scenarios (formation of a strongly bound wetting layer or no wetting layer formation at all) we observed several scenarios somewhere in between, where the formation and stability of one (or several) wetting layers depends on the coverage and temperature. All molecules showing these features in our work are of plate-like character. In the bulk phase these molecules typically crystallize by T-stacking with some contributions of π-stacking. One can easily anticipate that in the sub-monolayer regime the molecules will adopt a flaton configuration, which might even be the case for additional layers (due to dipole and π-π interaction), until T-stacked island structures become, due to quadrupole interactions, energetically more favorable. Such a phase transition has to be accompanied by a dewetting process. Indeed, dewetting, which is governed by coverage and temperature, is one of the crucial processes involved in the early stages of organic film growth [53,69]. This is probably one of the most undesirable features when it comes to application of such films in organic electronic devices.

A prime example showing the above described features is the plate-like molecule HATCN, deposited on Au(111) [43] and Ag(111) [47]. On Au(111) first a monolayer of strongly bound flat lying molecules develops. The corresponding desorption spectra show a decrease of the peak maxima with increasing coverage, again indicative of repulsive dipole forces between the adsorbed molecules. Further exposure leads to a second layer of flat-lying molecules. The binding energy of these molecules to the underlying molecules is much lower than that of the first layer and dipole repulsion is negligible, manifested in a sharp desorption peak at lower temperature. Further coverage increase would lead to flat-lying molecules in the third layer. However, this configuration (pure π-π stacking) is energetically unfavorable. Thus, nucleation centers of T-stacked clusters form in which the weakly bonded molecules in the second layer become incorporated by dewetting. With further exposure islands grow on top of the first monolayer. The situation is even more complex when HATCN is adsorbed on the more reactive Ag(111) surface. In this case, the molecules in the first wetting layer are so strongly bonded that they cannot be desorbed. With increasing coverage, however, these molecules reorient and a layer of standing molecules is formed [48]. Molecules in this layer can also not be desorbed in intact form, but C_2N_2 desorption is observed. Further exposure leads to a metastable layer on top of the first layer, composed of flaton and side-on oriented molecule. This molecule arrangement anticipates already the T-stacked bulk structure. Finally, adsorbed molecules in the third layer will initiate critical 3D T-stacked clusters, which induce rapid dewetting of the second layer, accompanied by 3D island growth.

In the above described systems the first layers were quite strongly bound and partial or full dewetting proceeded upon coverage and/or temperature increase. Another intermediate scenario can be observed on rather inert substrates, e.g. on silicon dioxide. Both, rubicene [50] and indigo molecules [54] adsorb in the sub-monolayer regime flat on the substrate, but exhibit a very low adsorption energy. Nevertheless, below a critical coverage this adsorbed phase is stable and no dewetting takes place. However, above a critical coverage suddenly dewetting sets in and 3D islands develop. Since the binding energy of the molecules in the (typically T-stacked) 3D islands is larger than between the monomers and the substrate surface, desorption of the multilayer proceeds at higher temperature than for the (sub)-monolayer. The critical dewetting coverage depends on the system. While this critical

coverage is about 1 monolayer for rubicene on SiO_2 it was observed to be about 2 monolayers on C-covered SiO_2. On the other hand, for indigo dewetting starts already at 0.25 ML on a C-covered SiO_2 surface, but above 1 ML on a sputter-cleaned surface.

A further potential of thermal desorption spectroscopy in the context of organic molecule adsorption and desorption is the capability to determine possible cracking processes during sample heating. The most frequently observed process is the decomposition of the first layers on reactive substrates, leading to a more or less carbon covered inert substrate. This decomposition, which is accompanied by hydrogen desorption, typically takes place at temperatures just above the desorption temperature of the monolayer. In the case of 4P and 6P adsorption on gold surfaces we observed that, in addition to complete decomposition, also partial decomposition, followed by cyclo-dimerisation, leads to more stable polycyclic hydrocarbons, which eventually decompose at even higher temperature [27,32]. Another example is the partial decomposition of side-on oriented HATCN molecules on Ag(111), which was accompanied by desorption of C_2N_2 [47].

Finally, TDS is the method of choice to get information on the adsorption and desorption kinetics. It is frequently assumed that organic molecules adsorb with a sticking coefficient of one on most substrates at room temperature and below. However, we could find several adsorption systems where a significantly smaller initial sticking coefficient was observed (e.g. $s_0 = 0.17$ for rubicene on SiO_2 [50]). Without going into details, our observations suggest that for flexible molecules (phenylenes) the initial sticking coefficient is close to one, while for stiff molecules (rubicene, pentacene) the initial sticking coefficient can be significantly smaller than one. With increasing coverage, sticking approaches the value of one in all cases. Several reasons for the low initial sticking and the increased sticking with coverage for stiff molecules can be suggested: (a) Stiff rod-like molecules approaching the (clean) surface head-on may not be able to rotate into the parallel adsorption geometry within the interaction time. (b) On the clean, stiff SiO_2 surface less kinetic energy can be transferred than on a surface already covered with soft matter, where low energy vibrational modes can be excited. (c) The impinging molecules may enter a precursor well where they can migrate over the surface for some time, before they desorb. At already adsorbed molecules or clusters they may be able to lose enough energy to become adsorbed. Unfortunately, there exists nearly no literature which addresses these issues for large organic molecules from a theoretical point of view, e.g. by molecular dynamics or Monte Carlo simulations. One can hope that the increasing number of quantitative experimental data and the ever-increasing computational power will encourage theoreticians to look in more detail into the fascinating issue of organic molecule adsorption.

Similarly, desorption of large organic molecules is only unsatisfactorily understood, and little theoretical work exists in this context [23,24]. In particular, desorption from the first (wetting) layers can be a quite complicated process. Since for large organic molecules many more degrees of freedom can be excited during desorption, than for small molecules or atoms, the desorption rate is to a much greater extent influenced by the entropic term than by the energetic term. Simple methods to estimate the desorption energy just from the maximum of the desorption peak (e.g. by the Redhead method [11]) can be very misleading. More refined methods, e.g. by variation of the heating rate might result in more reliable

results. On the other hand, desorption from the multilayer islands typically exhibit very clear zero-order desorption characteristic, and from quantitative TDS both, the desorption energy and the frequency factor, can be derived via the Polanyi–Wigner equation. One characteristic feature observed for desorption of all organic molecules is the very large frequency factor; typically much larger than the “classical” value of 10^{13} s^{-1}. A compilation of the frequency factors and desorption energies (heat of evaporation) calculated for multilayer desorption of the molecules investigated in this article is given in Table 1. The values for the frequency factors vary between 10^{18} s^{-1} and 10^{26} s^{-1}. Meanwhile, such large frequency factors for large organic molecule desorption have been reported in the literature several times [70,71]. The reasoning behind that is well understood by now. According to the transition state theory (TST) the frequency factor depends on the entropy change during desorption. i. e. on the ratio of the partition function in the transition state (which corresponds to the free state for non-activated adsorption) and the adsorbed state [19,21,22]. For large molecules the partition function is due to the many rotational and vibrational degrees of freedom much larger than for the adsorbed molecule, where only frustrated translations, rotations and vibrations exist.

Acknowledgments

The author gratefully acknowledges the main contributions to this review article by his former PhD students Stefan Müllegger, Paul Frank, Levent Tumbek and Boris Scherwitzl, as well as the helpful support by his colleagues Christian Teichert, Gregor Hlawacek, Roland Resel, Norbert Koch, Christof Wöll, and by many others. This research has been financially supported by several projects of the Austrian Science Fund (FWF): Project No. P 15625, P 19197, P 23530 and TRP 239.

References

[1]. Dimitrakopoulos CD, Malenfant PRL. Adv. Mater. 2002; 14:99.
[2]. Koch N. ChemPhysChem. 2007; 8:1438. [PubMed: 17539032]
[3]. Katz HE, Huang J. Annu. Rev. Mater. Res. 2009; 39:71.
[4]. Sirringhaus H. Adv. Mater. 2005; 17:2411.
[5]. Forrest SR. Chem. Rev. 1997; 97:1793. [PubMed: 11848893]
[6]. Heath JR. Annu. Rev. Mater. Res. 2009; 39:1.
[7]. Schreiber F. Prog. Surf. Sci. 2000; 65:151.
[8]. Horowitz G. J. Mater. Res. 2004; 19:1946.
[9]. O’Neill M, Kelly SM. Adv. Mater. 2011; 23:566. [PubMed: 21274907]
[10]. Lin P, Yan F. Adv. Mater. 2012; 24:34. [PubMed: 22102447]
[11]. Readhead PA. Vacuum. 1962; 12:203.
[12]. Rendulic KD, Winkler A. Surf. Sci. 1994; 299/300:261.
[13]. Müllegger S, Salzmann I, Resel R, Hlawacek G, Teichert C, Winkler A. J. Chem. Phys. 2004; 121:2272. [PubMed: 15260782]
[14]. Bondi A. J. Phys. Chem. 1964; 68:441.
[15]. Müllegger S, Salzmann I, Resel R, Winkler A. Appl. Phys. Lett. 2003; 83:4536.
[16]. Müllegger S, Hänel K, Strunskus T, Wöll C, Winkler A. ChemPhysChem. 2006; 7:2552. [PubMed: 17094155]
[17]. Menzel D. Desorption Phenomena, Topics in Applied Physics. 1975; 4:101.
[18]. King DA. Surf. Sci. 1975; 47:384.
[19]. Fichthorn KA, Becker KE, Miron RA. Catal. Today. 2007; 123:71.
[20]. Müllegger, S. PhD Thesis. Graz University of Technology; 2005.

[21]. Zhdanov VP. Surf. Sci. Rep. 1991; 12:183.
[22]. Kolasinski, KW. Surface Science. John Wiley & Sons; 2002.
[23]. Paserba KR, Gellman AJ. Phys. Rev. Lett. 2001; 86:4338. [PubMed: 11328169]
[24]. Fichthorn KA, Miron RA. Phys. Rev. Lett. 2002; 89:196103. [PubMed: 12443133]
[25]. Pfnür H, Feulner P, Engelhardt HA, Menzel D. Chem. Phys. Lett. 1978; 59:481.
[26]. Ibach H, Erley W, Wagner H. Surf. Sci. 1980; 92:29.
[27]. Müllegger S, Winkler A. Surf. Sci. 2006; 600:1290.
[28]. Müllegger S, Hlawacek G, Haber T, Frank P, Teichert C, Resel R, Winkler A. Appl. Phys. A. 2007; 87:103.
[29]. Opila P, Gomer R. Surf. Sci. 1981; 112:1.
[30]. Haber T, Müllegger S, Winkler A, Resel R. Phys. Rev. B. 2006; 74:045419.
[31]. Weiss K, Beernik G, Dötz F, Birkner A, Müllen K, Wöll C. Angew. Chem. Int. Ed. 1999; 38:3748.
[32]. Müllegger S, Winkler A. Surf. Sci. 2006; 600:3982.
[33]. Andreev AY, Matt G, Sitter H, Brabec CJ, Badt D, Neugebauer H, Sariciftci NS. Synth. Met. 2001; 116:235.
[34]. Balzer F, Rubahn HG. Surf. Sci. 2002; 507:588.
[35]. Schieck M, Balzer F, Al-Shamery K, Brewer JR, Lützen A, Rubahn HG. Small. 2008; 4:176. [PubMed: 18203230]
[36]. Frank P, Hlawacek G, Lengyel O, Satka A, Teichert C, Resel R, Winkler A. Surf. Sci. 2007; 601:2152.
[37]. Resel R, Haber T, Lengyel O, Balzer F, Rubahn HG. Surf. Interface Anal. 2009; 41:764.
[38]. Müller K, Chang CC. Surf. Sci. 1969; 14:39.
[39]. Balzer F, Rubahn HG. Appl. Phys. Lett. 2001; 79:3860.
[40]. Ehrlich G, Hudda FG. J. Chem. Phys. 1966; 44:1039.
[41]. Schwoebel RL, Shipsey EJ. J. Appl. Phys. 1966; 37:3682.
[42]. Glowatzki H, Bröcker B, Blum RP, Hofmann OT, Vollmer A, Rieger R, Müllen K, Zojer E, Raabe JP, Koch N. Nano Lett. 2008; 8:3825. [PubMed: 18954123]
[43]. Frank P, Koch N, Koini M, Rieger R, Müllen K, Resel R, Winkler A. Chem. Phys. Lett. 2009; 473:321.
[44]. Polta JA, Thiel PA. J. Am. Chem. Soc. 1986; 108:7560. [PubMed: 22283258]
[45]. Jakob P, Menzel D. Surf. Sci. 1989; 220:70.
[46]. Szalay PS, Galán-Mascaros JR, Clérac R, Dunbar KR. Synth. Met. 2001; 122:535.
[47]. Frank P, Djuric T, Koini M, Salzmann I, Rieger R, Müllen K, Resel R, Koch N, Winkler A. J. Phys. Chem. C. 2010; 114:6650.
[48]. Bröcker B, Hofmann OT, Rangger GM, Frank P, Blum RP, Rieger R, Venema L, Vollmer A, Müllen K, Rabe JP, Winkler A, Rudolf P, Zojer E, Koch N. Phys. Rev. Lett. 2010; 104:246805. [PubMed: 20867325]
[49]. Bridge ME, Marbrow RA, Lambert RM. Surf. Sci. 1976; 57:415.
[50]. Scherwitzl B, Lukesch W, Hirzer A, Albering J, Leising G, Resel R, Winkler A. J. Phys. Chem. C. 2013; 117:4115.
[51]. Tumbek L, Gleichweit C, Zojer K, Winkler A. Phys. Rev. B. 2012; 86:085402.
[52]. Irimia-Vladu M, Glowacki ED, Troshin PA, Schwabegger G, Leonat L, Susarova DK, Krystal O, Ullah M, Kanbur Y, Bodea MA, Razumov VF, Sitter H, Bauer S, Sariciftci NS. Adv. Mater. 2012; 24:375. [PubMed: 22109816]
[53]. Irimia-Vladu M, Glowacki ED, Voss G, Bauer S, Sariciftci NS. Mater. Today. 2012; 15:340.
[54]. Scherwitzl B, Resel R, Winkler A. J. Chem. Phys. 2014; 140:184705. [PubMed: 24832297]
[55]. Mitsui T, Rose MK, Fomin E, Ogletree DF, Salmeron M. Science. 2002; 297:1850. [PubMed: 12228712]
[56]. Ranea VA, Michaelides A, Ramírez R, de Andres PL, Vergés JA, King DA. Phys. Rev. Lett. 2004; 92:136104. [PubMed: 15089633]

[57]. Eichberger M, Marschall M, Reichert J, Weber-Bargioni A, Auwärter W, Wang RLC, Kreuzer HJ, Pennec Y, Schiffrin A, Barth JV. Nano Lett. 2008; 8:4608. [PubMed: 19367979]
[58]. Hlawacek G, Teichert C. J. Phys. Condens. Matter. 2013; 25:143202. [PubMed: 23478790]
[59]. Burke SA, Topple JM, Grütter P. J. Phys. Condens. Matter. 2009; 21:423101. [PubMed: 21715835]
[60]. Yang J, Yan D. Chem. Soc. Rev. 2009; 38:2634. [PubMed: 19690743]
[61]. Tautz FS. Prog. Surf. Sci. 2007; 82:479.
[62]. Witte G, Wöll C. J. Mater. Res. 2004; 19:1889.
[63]. Fraxedas J. Adv. Mater. 2002; 14:1603.
[64]. Baker KN, Fratini AV, Resch T, Knachel HC, Adams WW, Socci EP, Farmer BL. Polymer. 1993; 34:1571.
[65]. Venables JA, Spiller GDT, Hanbücken M. Rep. Prog. Phys. 1984; 47:399.
[66]. Tumbek L, Winkler A. Surf. Sci. Lett. 2012; 606:L55.
[67]. Frank P, Hernandez-Sosa G, Sitter H, Winkler A. Thin Solid Films. 2008; 516:2939.
[68]. Hlawacek G, Puschnig P, Frank P, Winkler A, Ambrosch-Draxl C, Teichert C. Science. 2008; 321:108. [PubMed: 18599783]
[69]. Käfer D, Wöll C, Witte G. Appl. Phys. A. 2009; 95:273.
[70]. Paserba KR, Vaidyanathan N, Gellman AJ. Langmuir. 2002; 18:9799.
[71]. Roos M, Breitruck A, Hoster HE, Behm RJ. Phys. Chem. Chem. Phys. 2010; 12:818. [PubMed: 20066366]

Europe PMC Funders Author Manuscripts

Europe PMC Funders Author Manuscripts

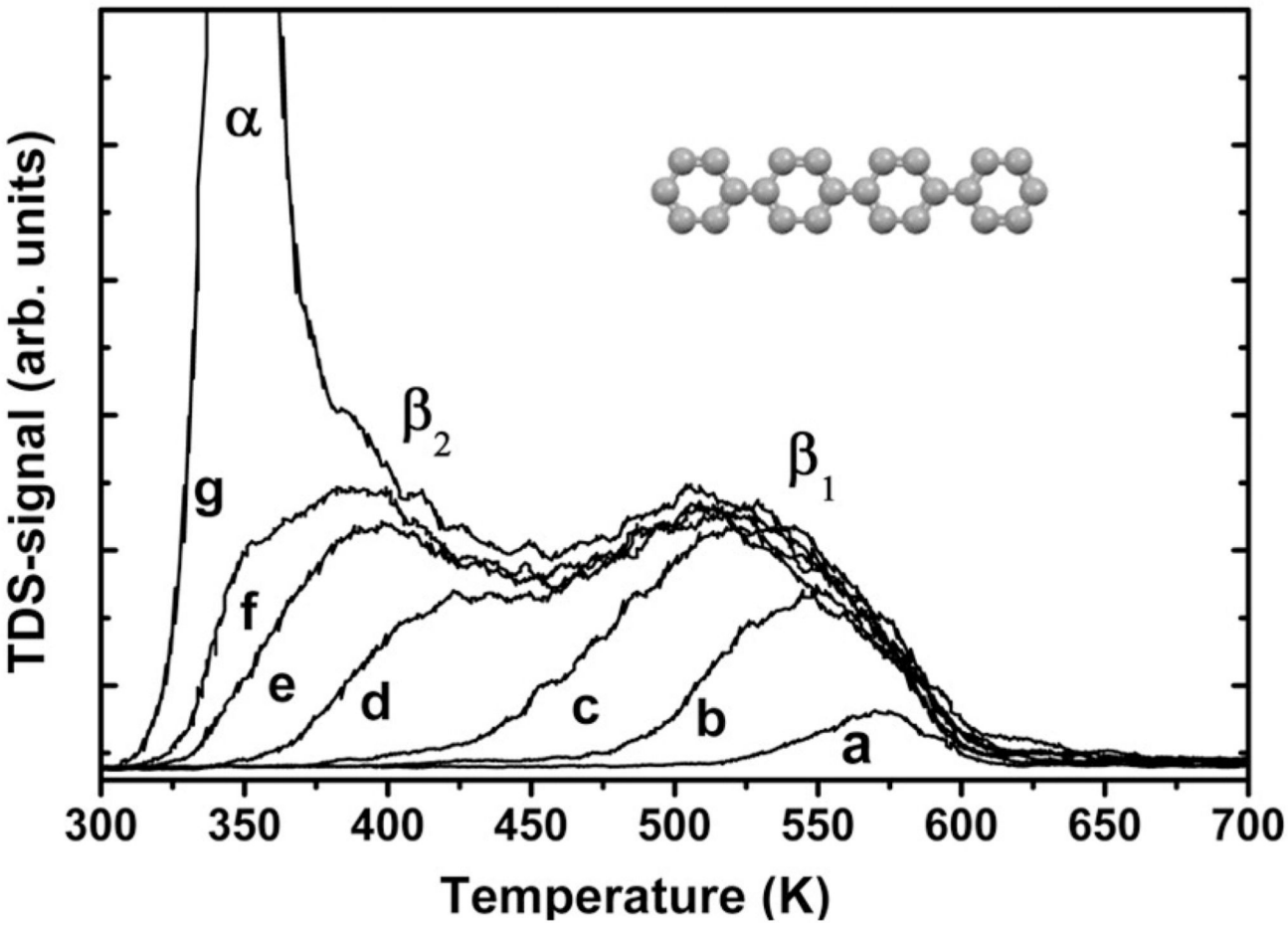

Fig. 1.

Series of TD spectra of 4P on Au(111) for different initial coverages (a) 0.02 nm-(g) 0.5 nm, adsorbed at 93 K. Heating rate: 1 K/s. The full mass m = 306 amu was detected. The multilayer peak is denoted as α. The monolayer is composed of two states which saturate at a mean thickness of 0.15 nm (trace (c) denoted $ß_1$) and 0.28 nm (trace (f) denoted $ß_2$), respectively. Chemical structure shown in the insert. (Adapted with permission from Ref. [13]).

Europe PMC Funders Author Manuscripts

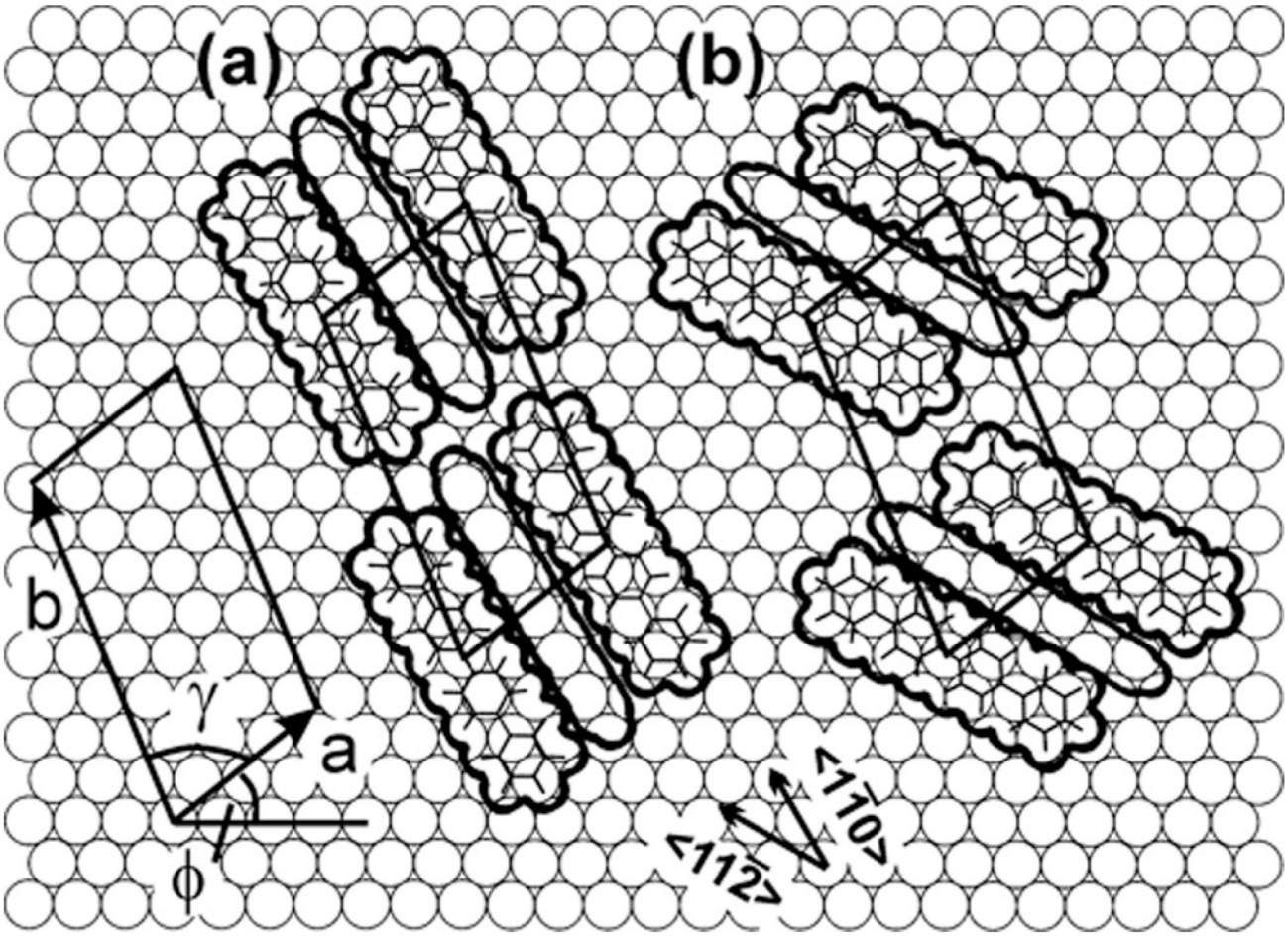

Fig. 2.

Real space representation of the saturated 4P monolayer surface unit cell on a Au(111) surface. Two different possible epitaxial arrangements of the 4P molecules relative to the Au surface atoms are shown. (Reprinted with permission from Ref. [13,15]).

Europe PMC Funders Author Manuscripts

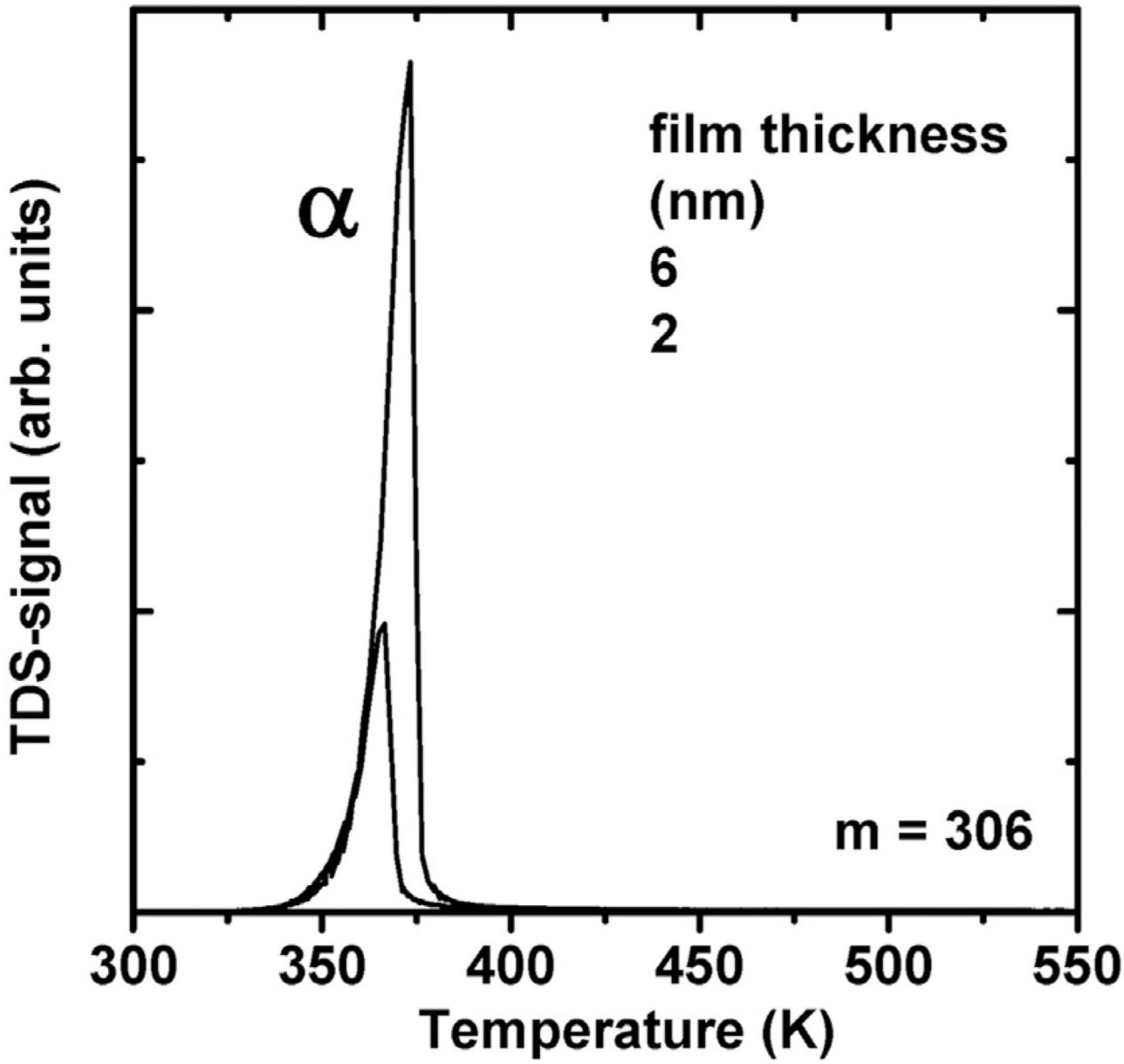

Fig. 3.

Multilayer desorption spectra of 4P from Au(111) for mean thicknesses of 2 and 6 nm, respectively. The full mass m = 306 amu was detected. Adsorption temperature: 93 K, heating rate: 1 K/s. [20].

Europe PMC Funders Author Manuscripts

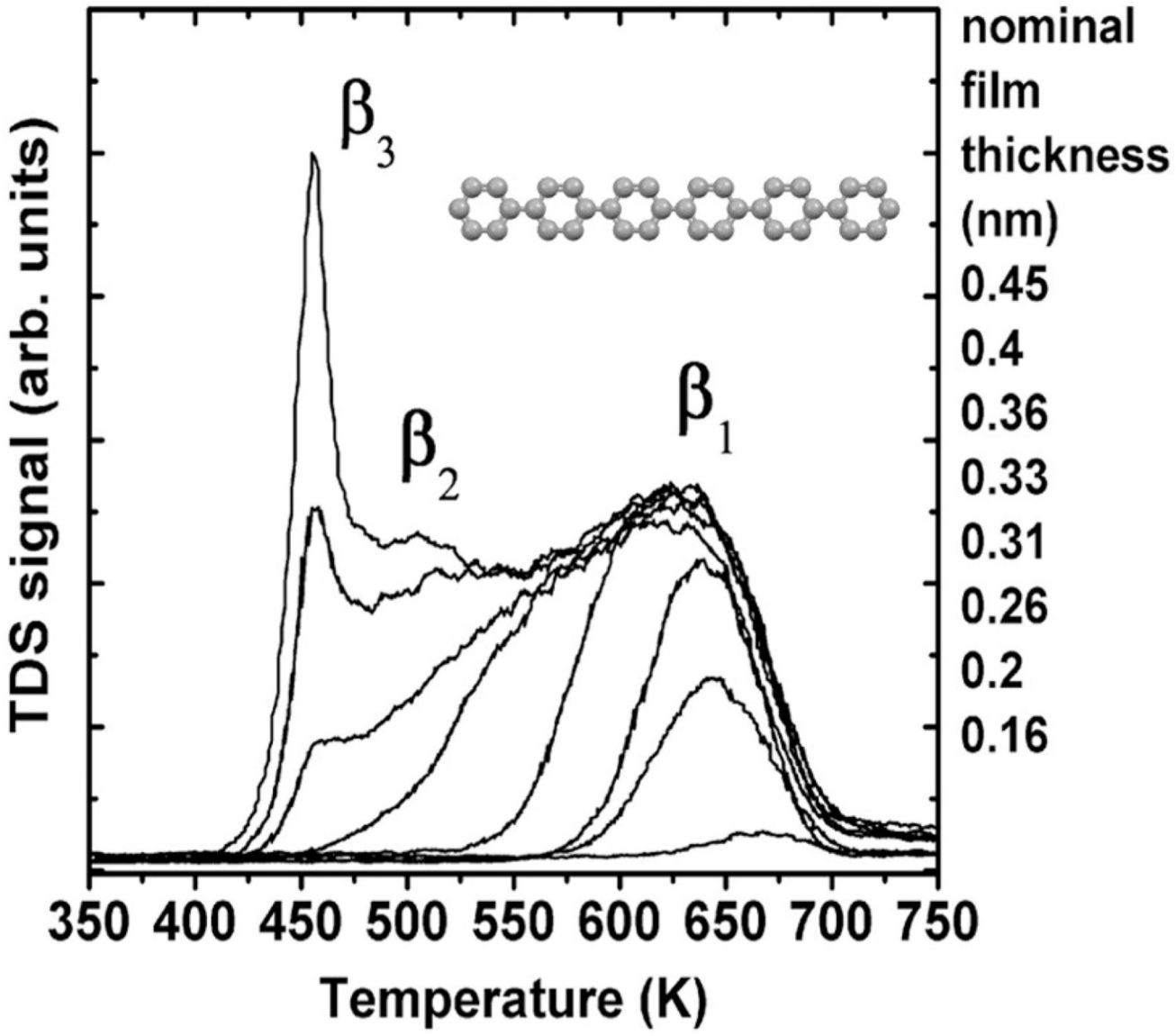

Fig. 4.

Series of TD spectra of 6P on Au(111) for different initial coverages (a) 0.16 nm–(g) 0.45 nm, adsorbed at 300 K. The cracking mass m = 61 amu was detected. Heating rate: 1 K/s. Chemical structure shown in the insert. (Adapted with permission from Ref. [27]).

Europe PMC Funders Author Manuscripts

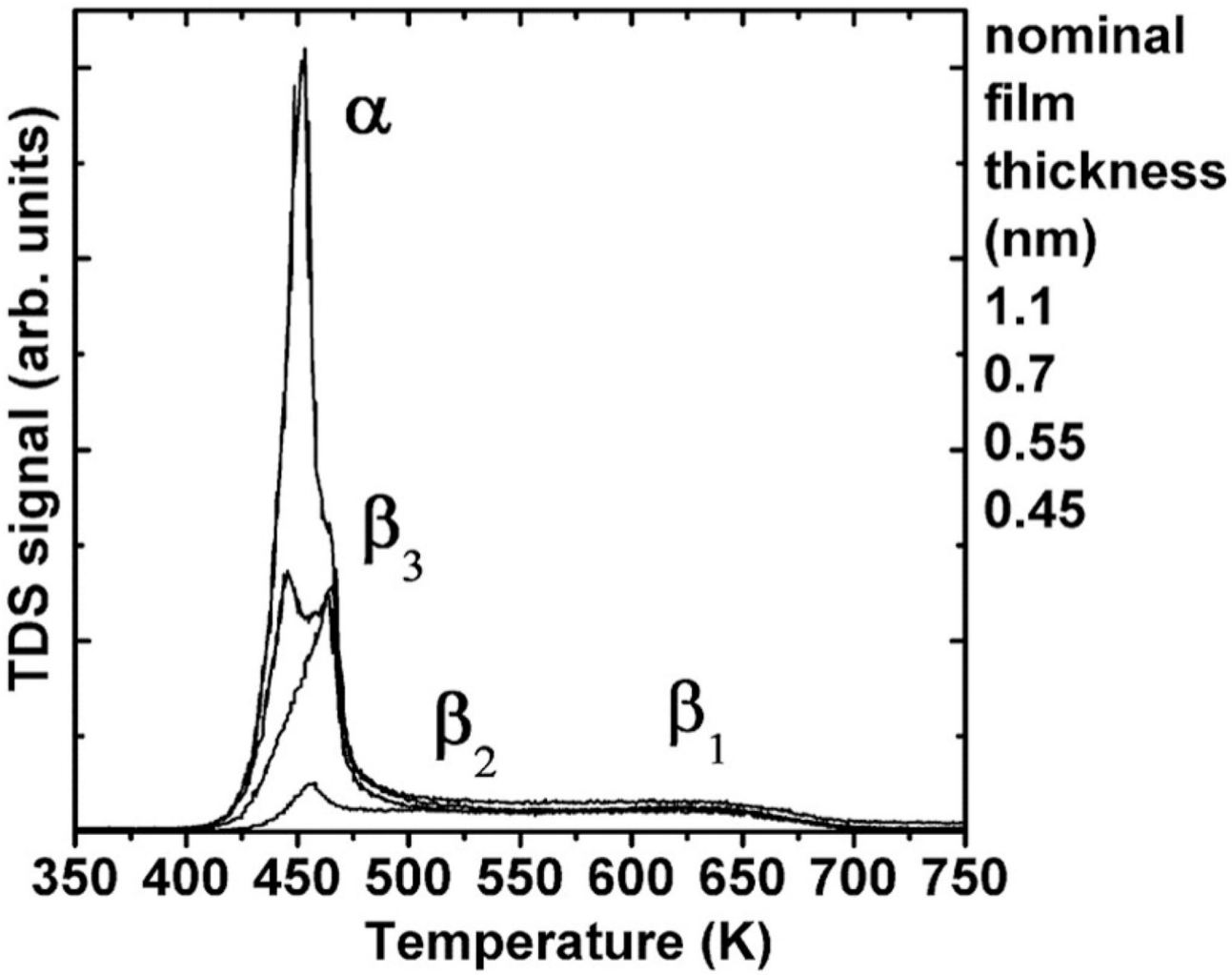

Fig. 5.

Series of TD spectra of 6P on Au(111) for coverages between 0.45 nm and 1.1 nm mean thickness, adsorbed at 300 K. The cracking mass m = 61 amu was detected. Heating rate: 1 K/s. (Reprinted with permission from Ref. [27]).

Europe PMC Funders Author Manuscripts

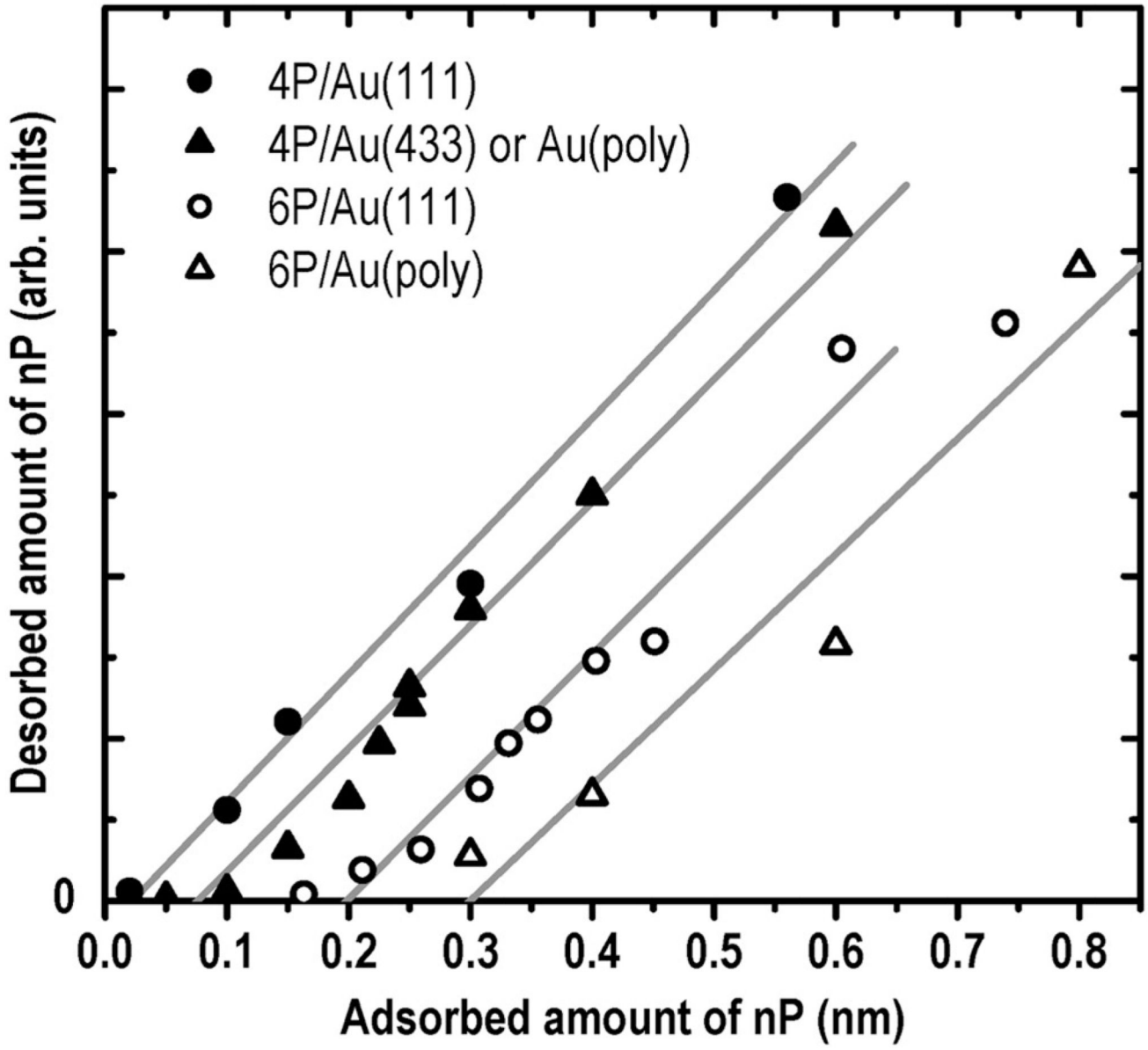

Fig. 6.

Compilation of TD data showing the desorbed vs. adsorbed amount of nP from different Au surfaces. The gray lines represent linear fits to the individual data sets. (Reprinted with permission from Ref. [32]).

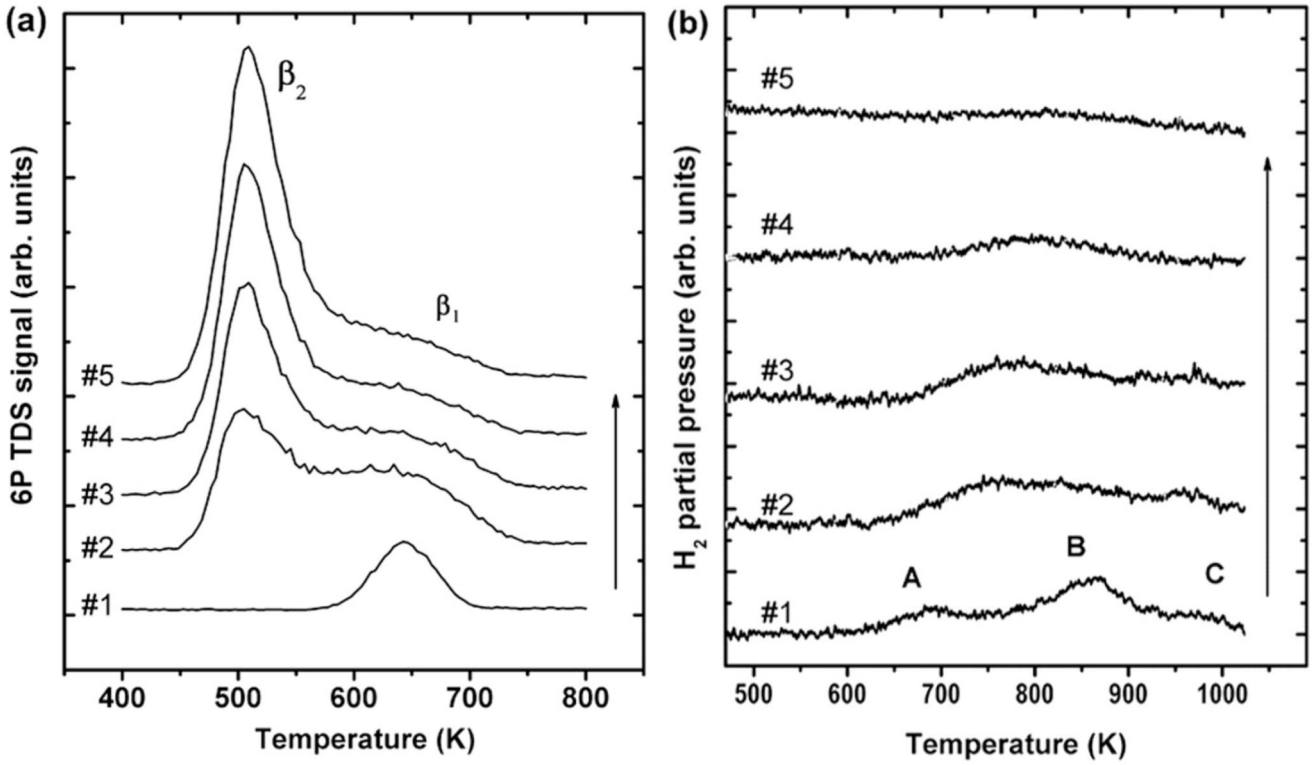

Fig. 7.

Desorption spectra of 6P (m = 61 amu) (a) and H_2 (m = 2 amu) (b) obtained from Au(111), starting with an initially clean surface, after deposition of 0.2 nm 6P at 300 K (trace #1), followed by further adsorption/desorption cycles with the same deposited amount (trace #2-#5). No substrate cleaning between cycles was performed (Reprinted with permission from Ref. [27]).

Europe PMC Funders Author Manuscripts

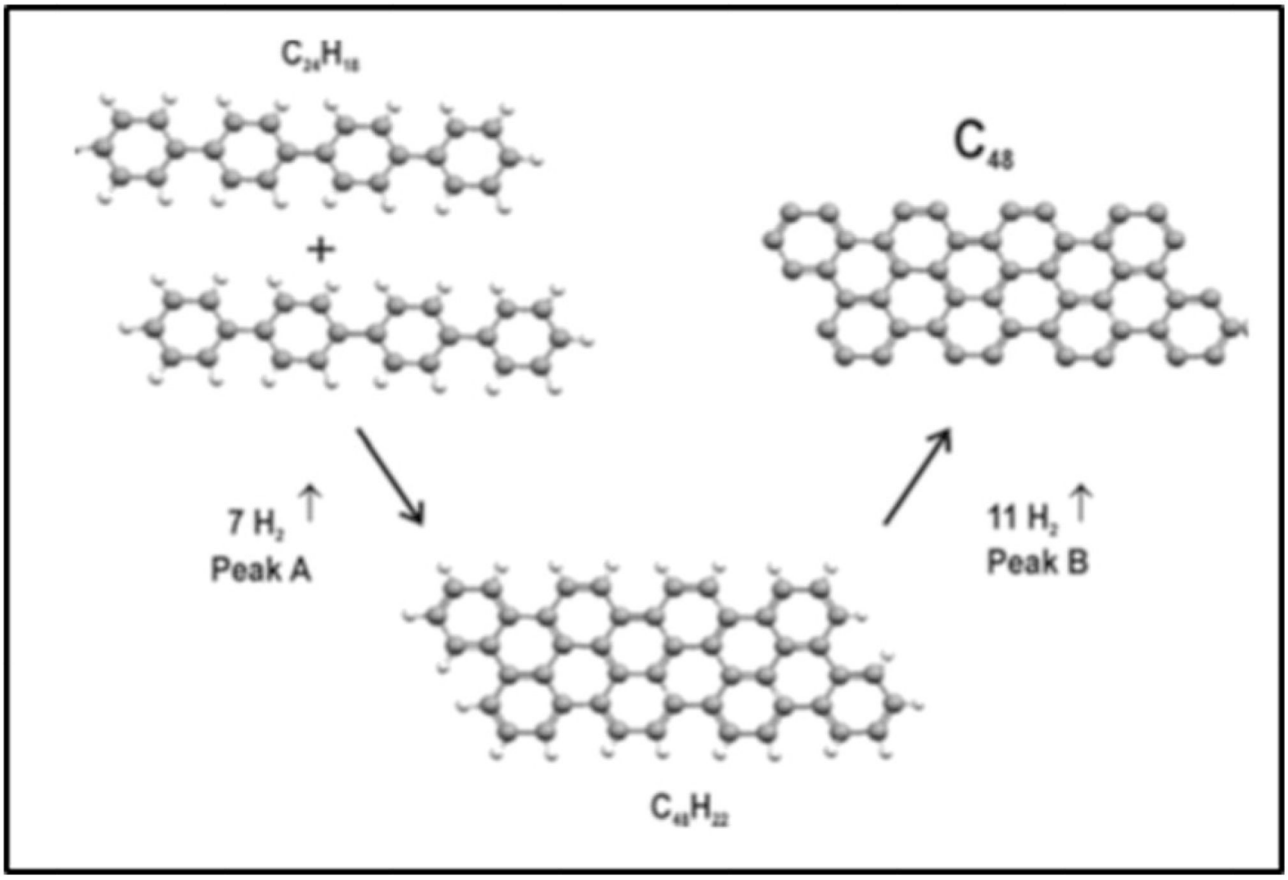

Fig. 8.

Proposed scenario for dehydrogenation/cyclo-dimerization of quaterphenyl. (Reprinted with permission from Ref. [32]).

Europe PMC Funders Author Manuscripts

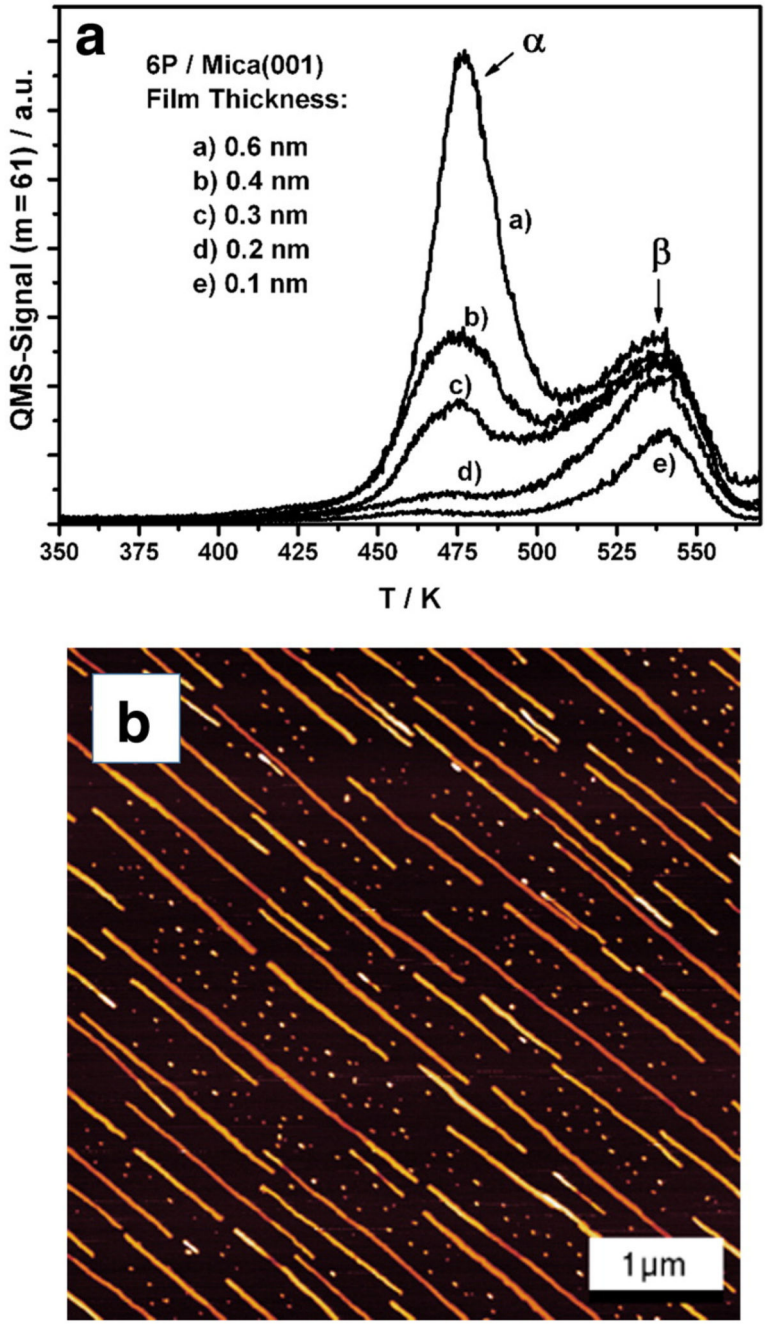

Fig. 9.

(a) TDS series of 6P grown on air cleaved mica(001) at 300 K. Heating rate: 1 K/s. The monolayer and multilayer desorption peaks are denoted ß and α, respectively. (b) AFM image of a 1 nm thick 6P film on air cleaved mica(001). (Reproduced with permission from Ref. [36]).

Europe PMC Funders Author Manuscripts

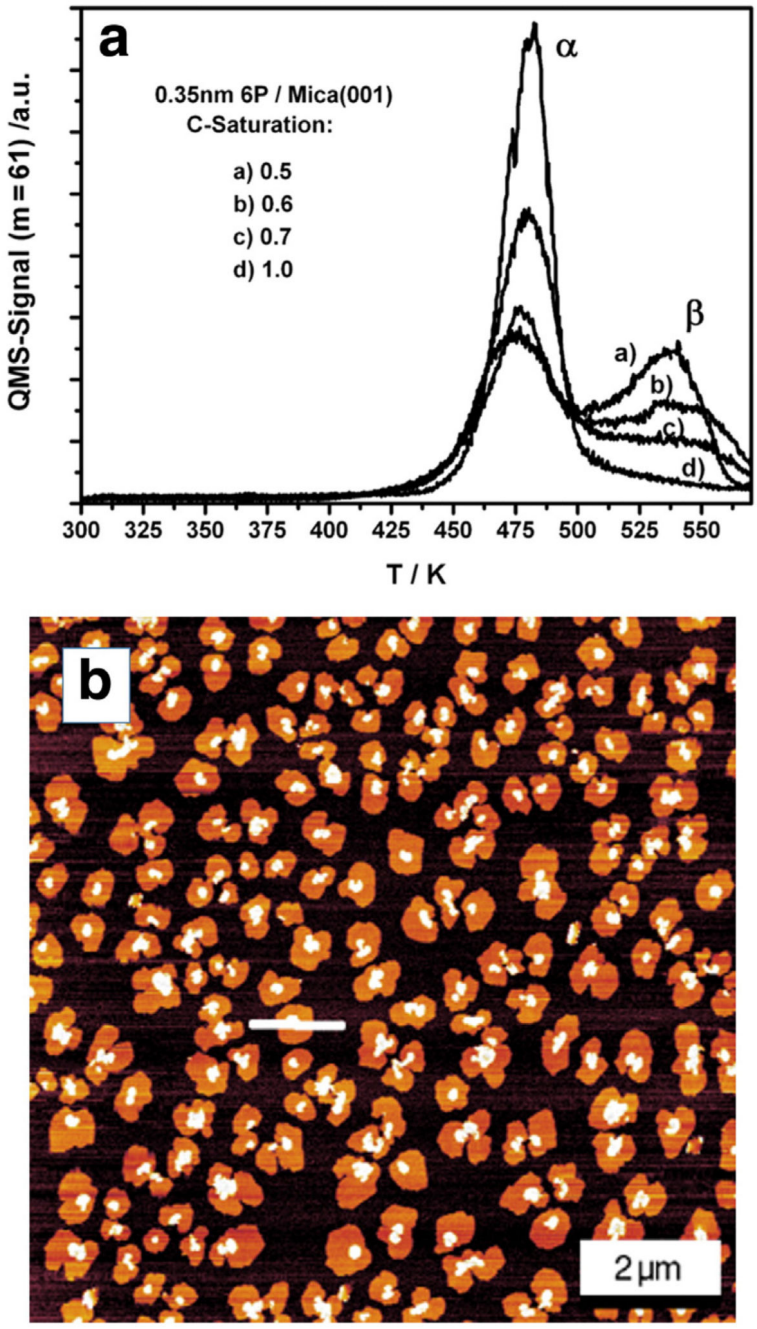

Fig. 10.

(a) TDS series of 0.35 nm 6P grown on partially C covered mica(001) at 300 K. Heating rate: 1 K/s. The monolayer and multilayer desorption peaks are denoted ß and α, respectively. (b) AFM image of a 1 nm thick 6P film on mica(001) covered with 1 monolayer of carbon. (Reproduced with permission from Ref. [36]).

Europe PMC Funders Author Manuscripts

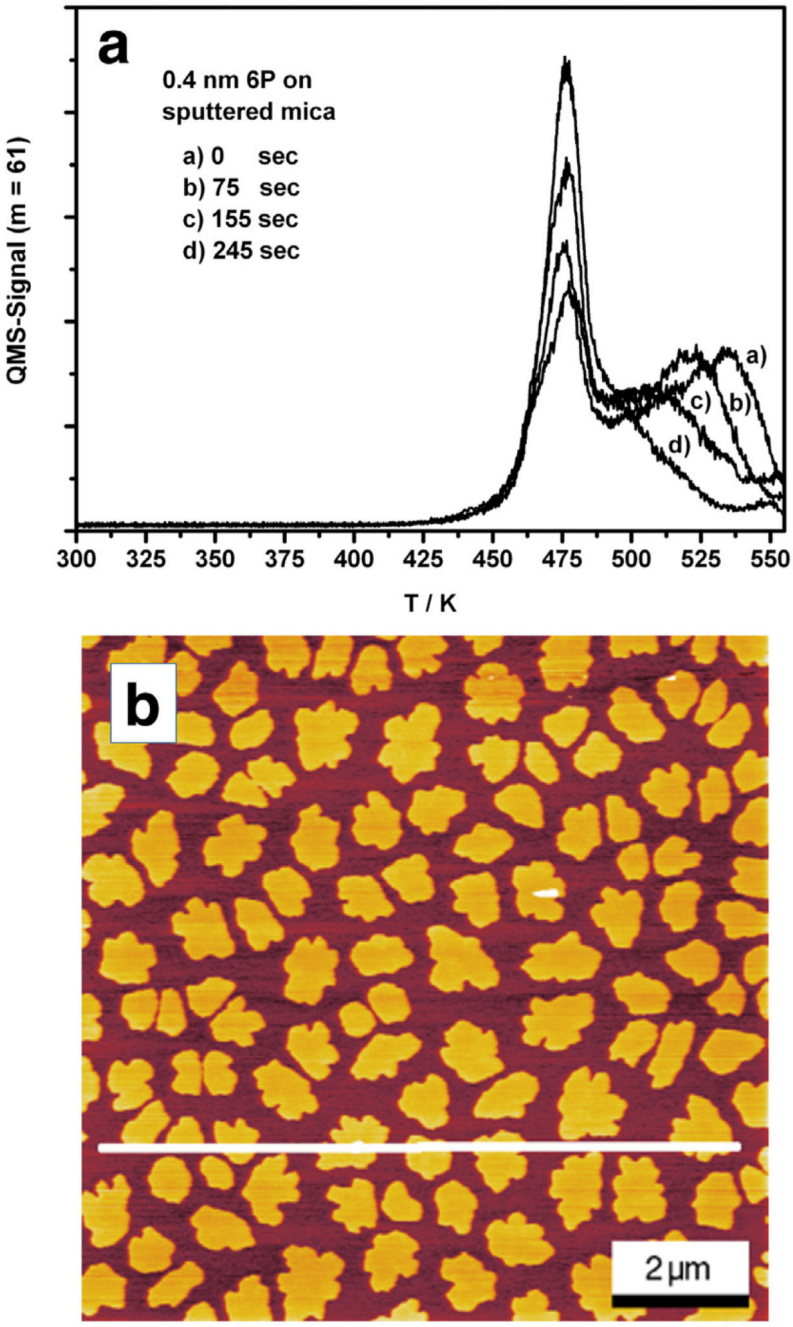

Fig. 11.

(a) TDS series of 0.4 nm 6P grown on mica(001) at 300 K after different sputter times. Heating rate: 1 K/s. (b) AFM image of a 1 nm thick 6P film grown on mica(001) after 245 s sputter time. (Reproduced with permission from Ref. [36]).

Europe PMC Funders Author Manuscripts

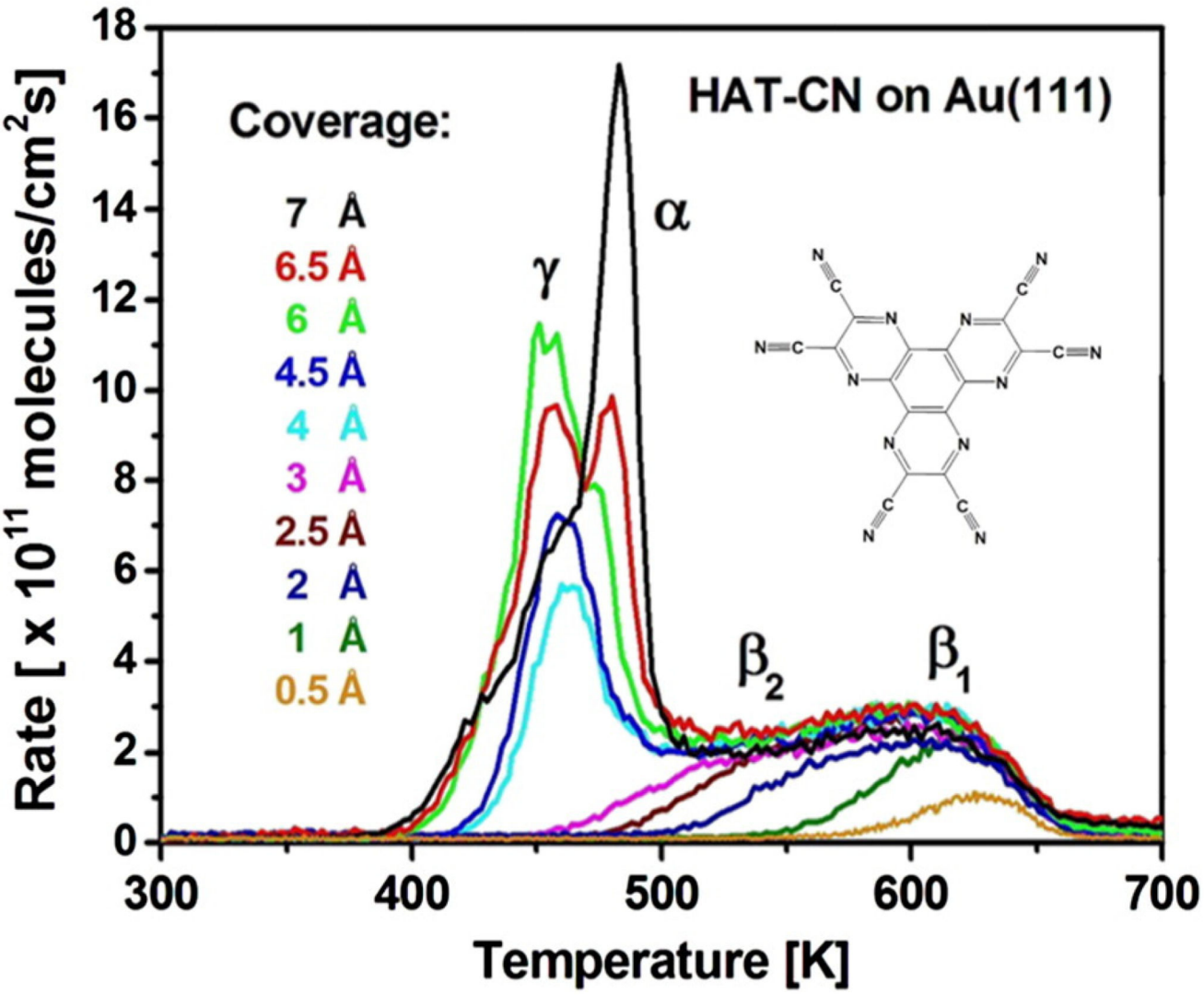

Fig. 12.

Series of thermal desorption spectra of HATCN on Au(111) as a function of coverage. Adsorption temperature: 200 K, heating rate: 1 K/s. The cracking mass m = 100 amu was detected. The chemical structure of HATCN is shown in the insert. (Reproduced with permission from Ref. [43]).

Europe PMC Funders Author Manuscripts

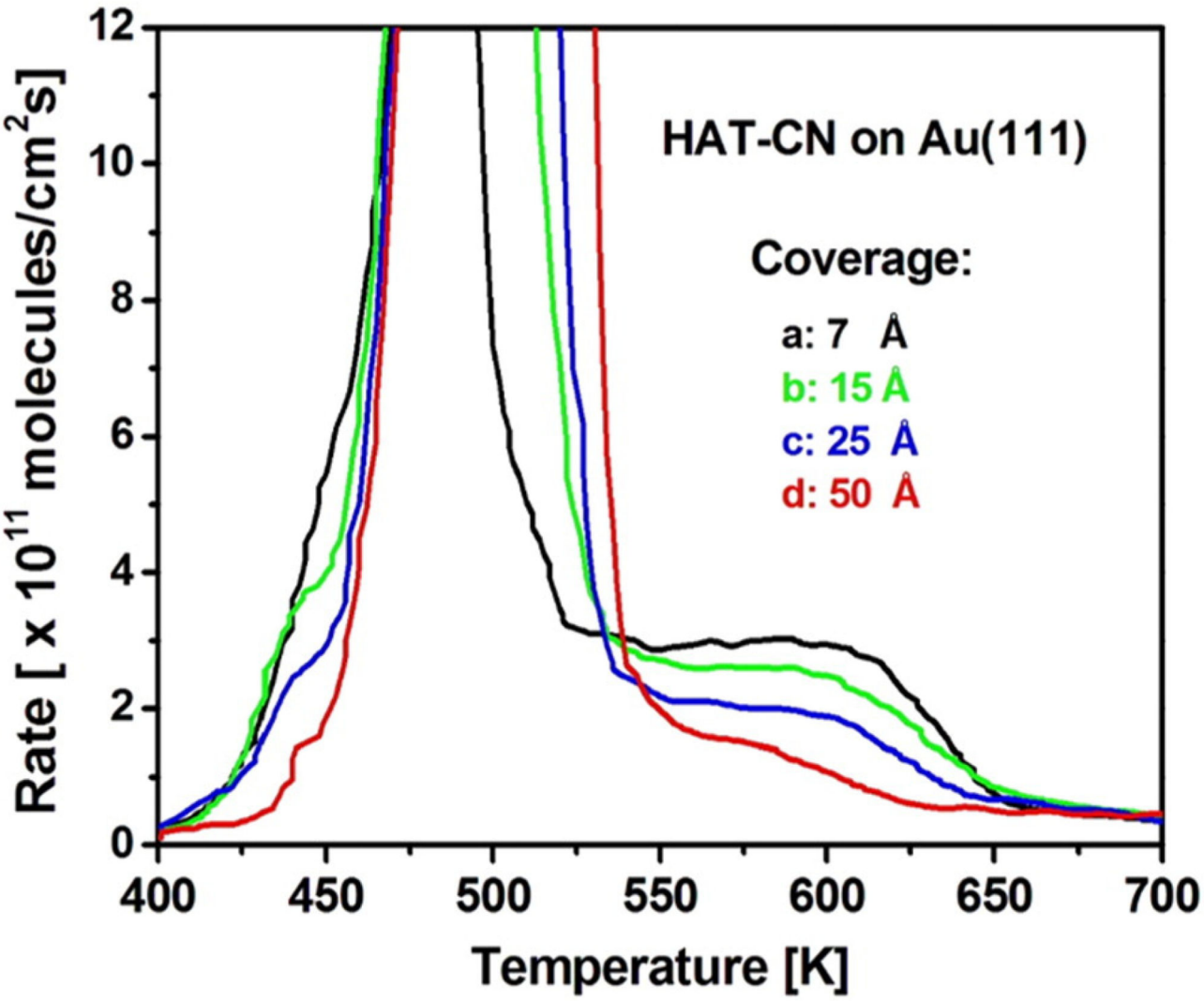

Fig. 13.

Series of desorption spectra of HATCN on Au(111) for larger coverages. T_{ads} = 200 K, heating rate: 1 K/s. The cracking mass m = 100 amu was detected. (Reproduced with permission from Ref. [43]).

Europe PMC Funders Author Manuscripts

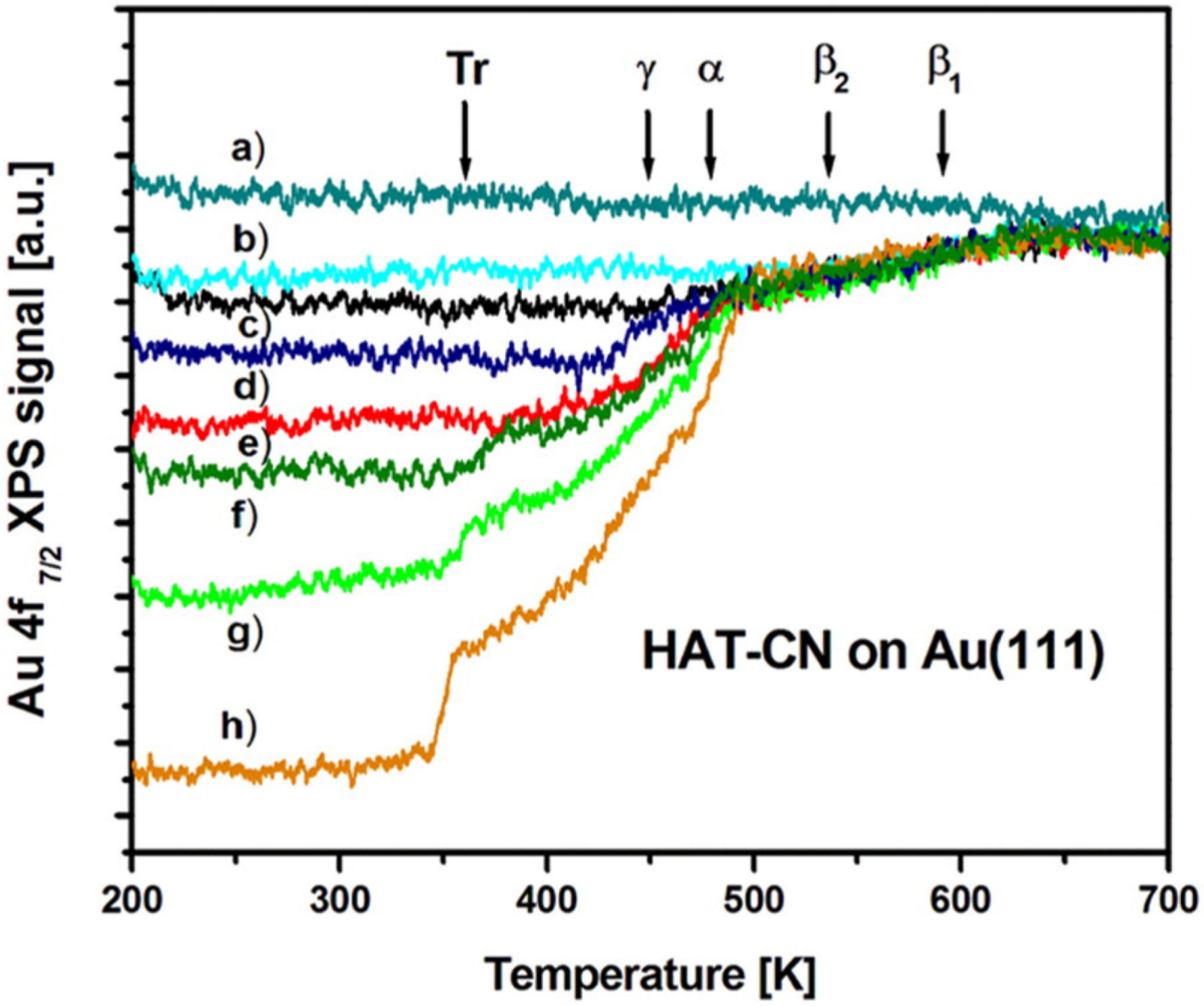

Fig. 14.

XPS Au4$f_{7/2}$ substrate signal change during heating of the sample, for various initial HATCN coverages. (a) 0 nm, (b) 0.2 nm, (c) 0.3 nm, (d) 0.5 nm, (e) 0.7 nm, (f) 0.8 nm, (g) 1 nm, (h) 1.5 nm. T_{ads}: 200 K, heating rate: 1 K/s. The peak maxima of the corresponding desorption peaks are indicated. (Reproduced with permission from Ref. [43]).

Europe PMC Funders Author Manuscripts

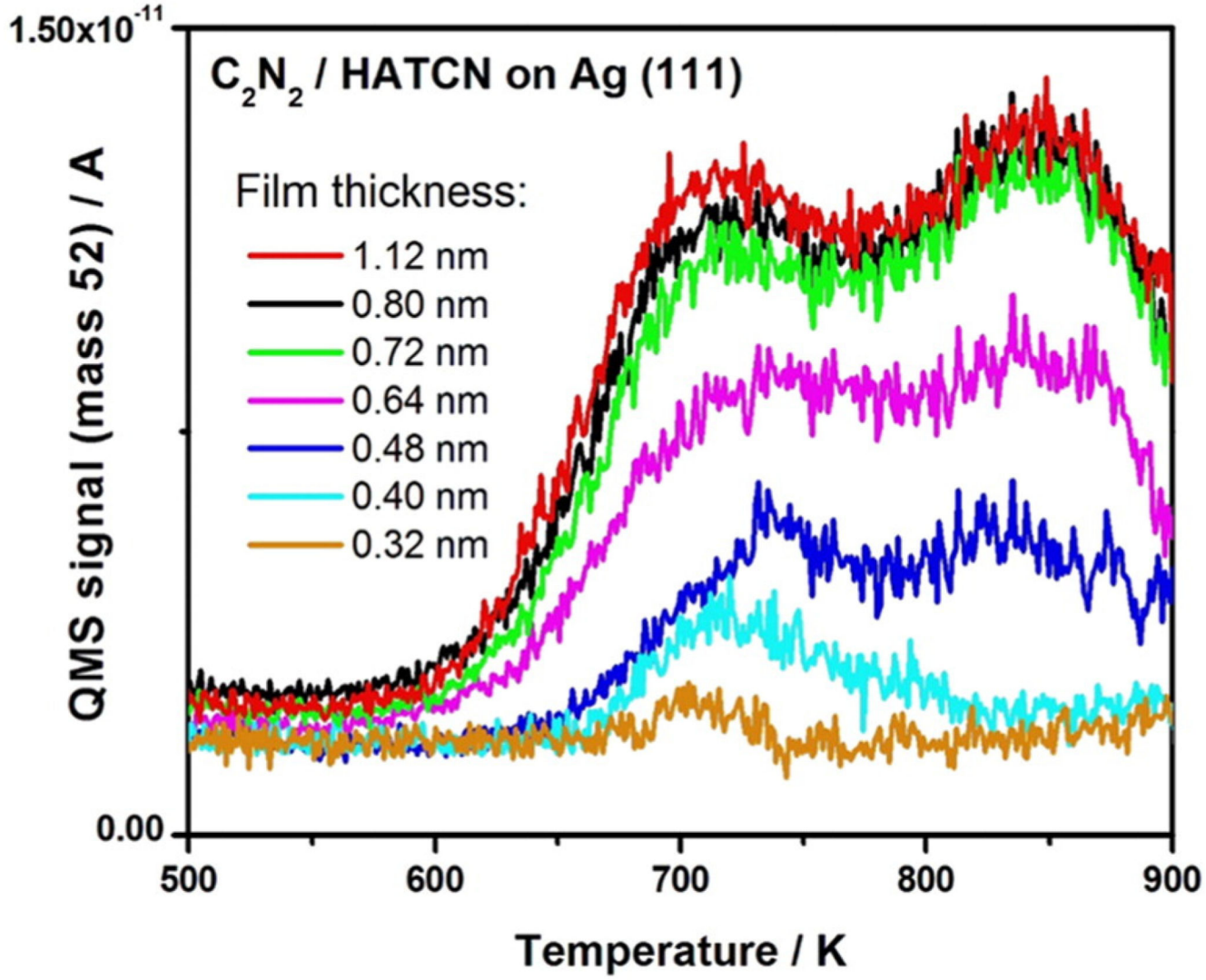

Fig. 15.

Desorption traces of mass 52 amu after adsorption of HATCN on Ag(111) at room temperature, up to 1.12 mean thickness. Heating rate: 1 K/s. No desorption of the intact molecules was observed in this coverage regime. (Reproduced with permission from Ref. [47]).

Europe PMC Funders Author Manuscripts

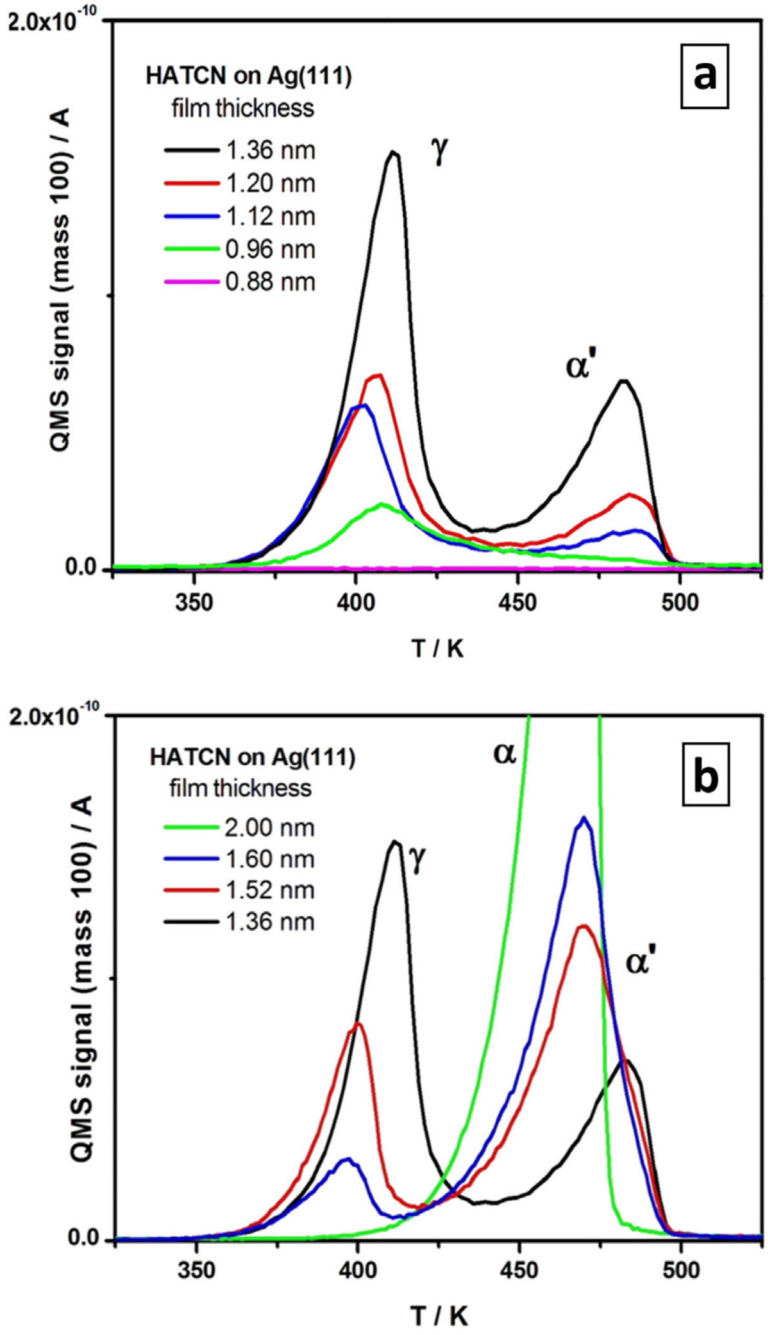

Fig. 16.

Series of TD spectra for HATCN from Ag(111) after adsorption at 300 K, for the coverage range 0.88 nm–1.36 nm (a) and 1.36 nm–2.0 nm (b). Heating rate 1 K/s. (Reproduced with permission from Ref. [47]).

Europe PMC Funders Author Manuscripts

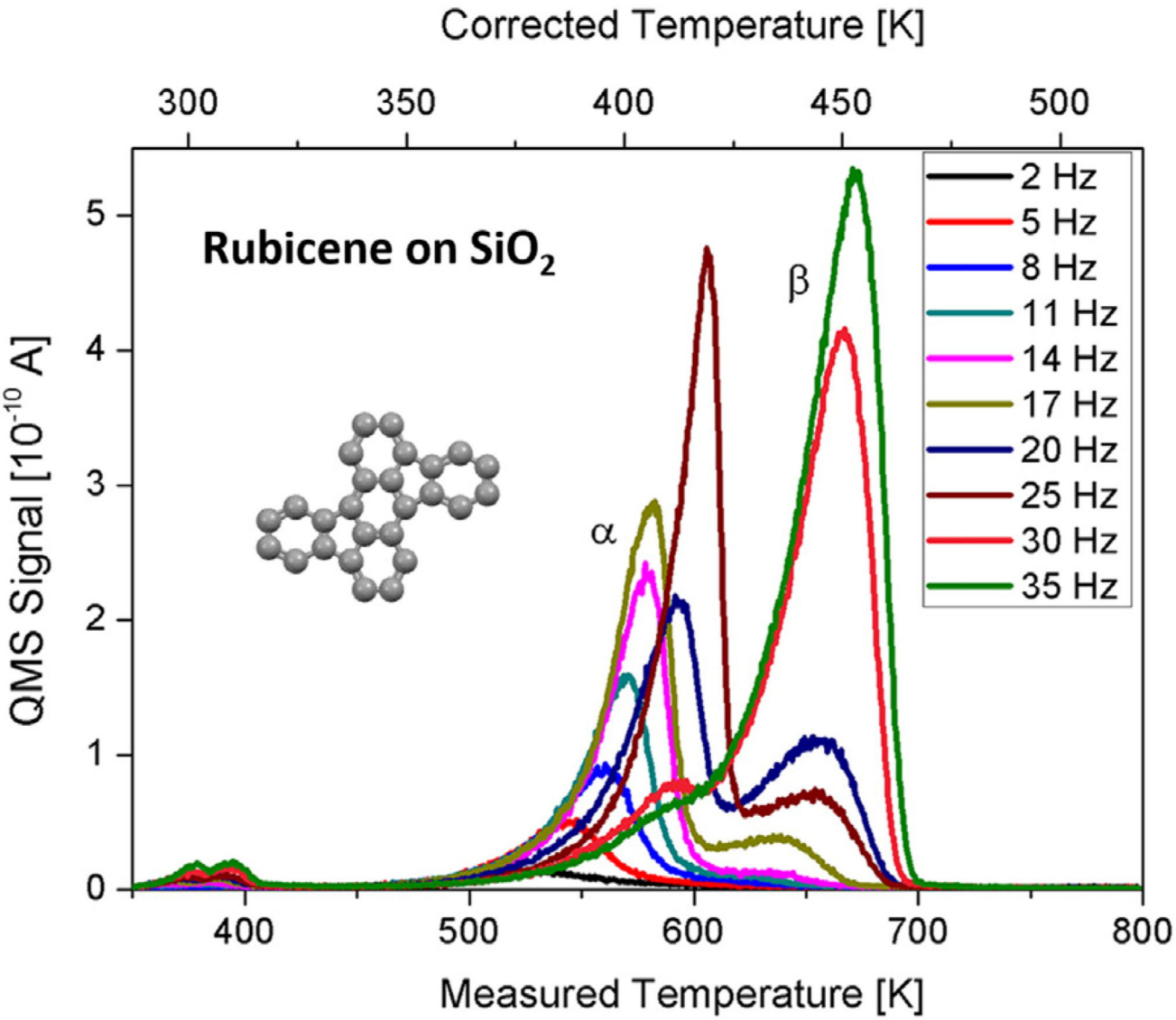

Fig. 17.

Thermal desorption spectra of rubicene from clean silicon dioxide for different exposures. T_{ads} = 220 K, heating rate ß = 1 K/s. The cracking mass m = 163 amu was detected. The exposure is given in Hz, as determined by a quartz microbalance. 1 Hz corresponds to 0.09 nm. (Adapted with permission from Ref. [50]).

Europe PMC Funders Author Manuscripts

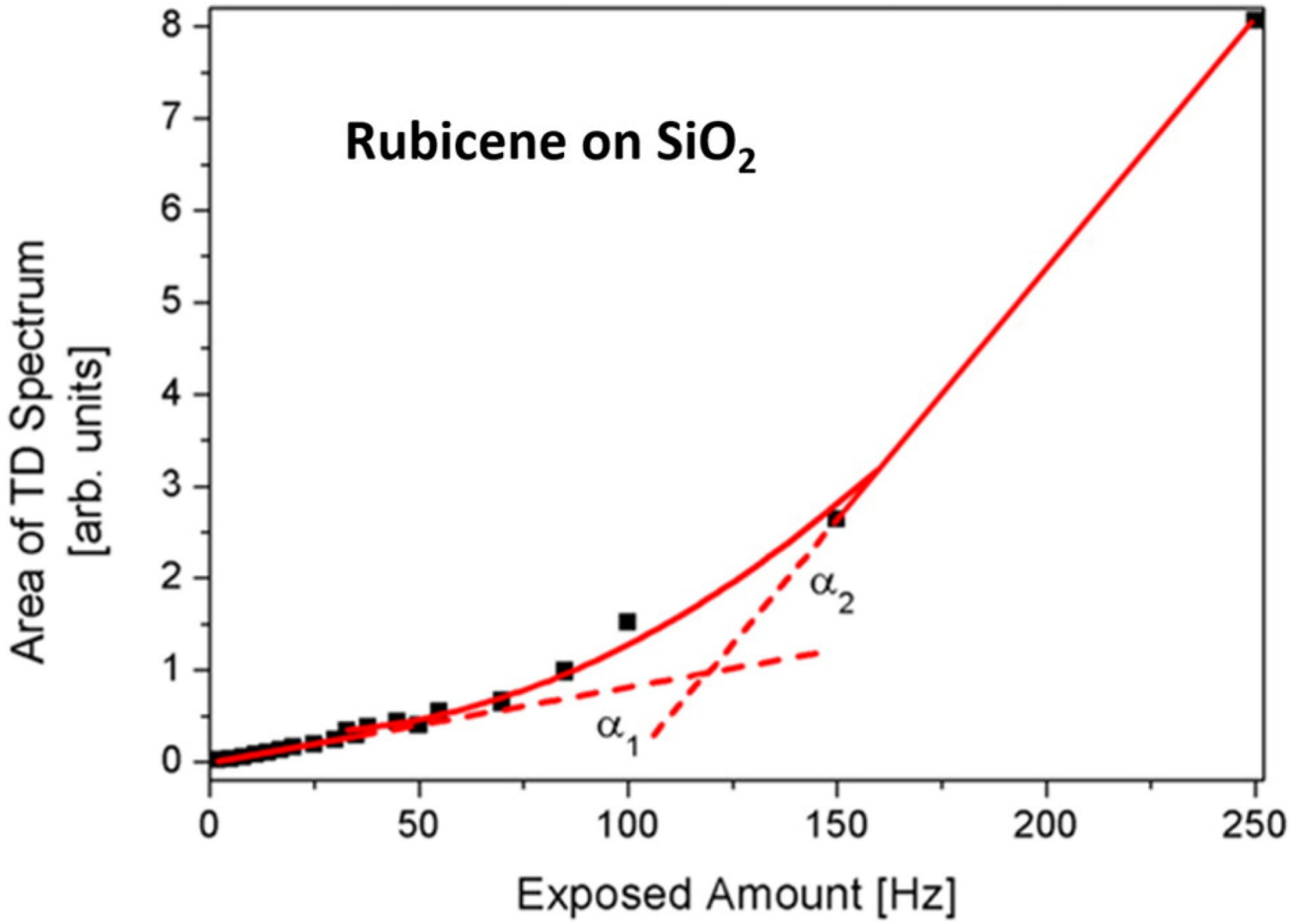

Fig. 18.

TDS areas for rubicene desorbed from sputter cleaned silicon dioxide as a function of the exposed amount, as measured by the quartz microbalance. Adsorption temperature: 220 K. (Reproduced with permission from Ref. [50], supporting material).

Europe PMC Funders Author Manuscripts

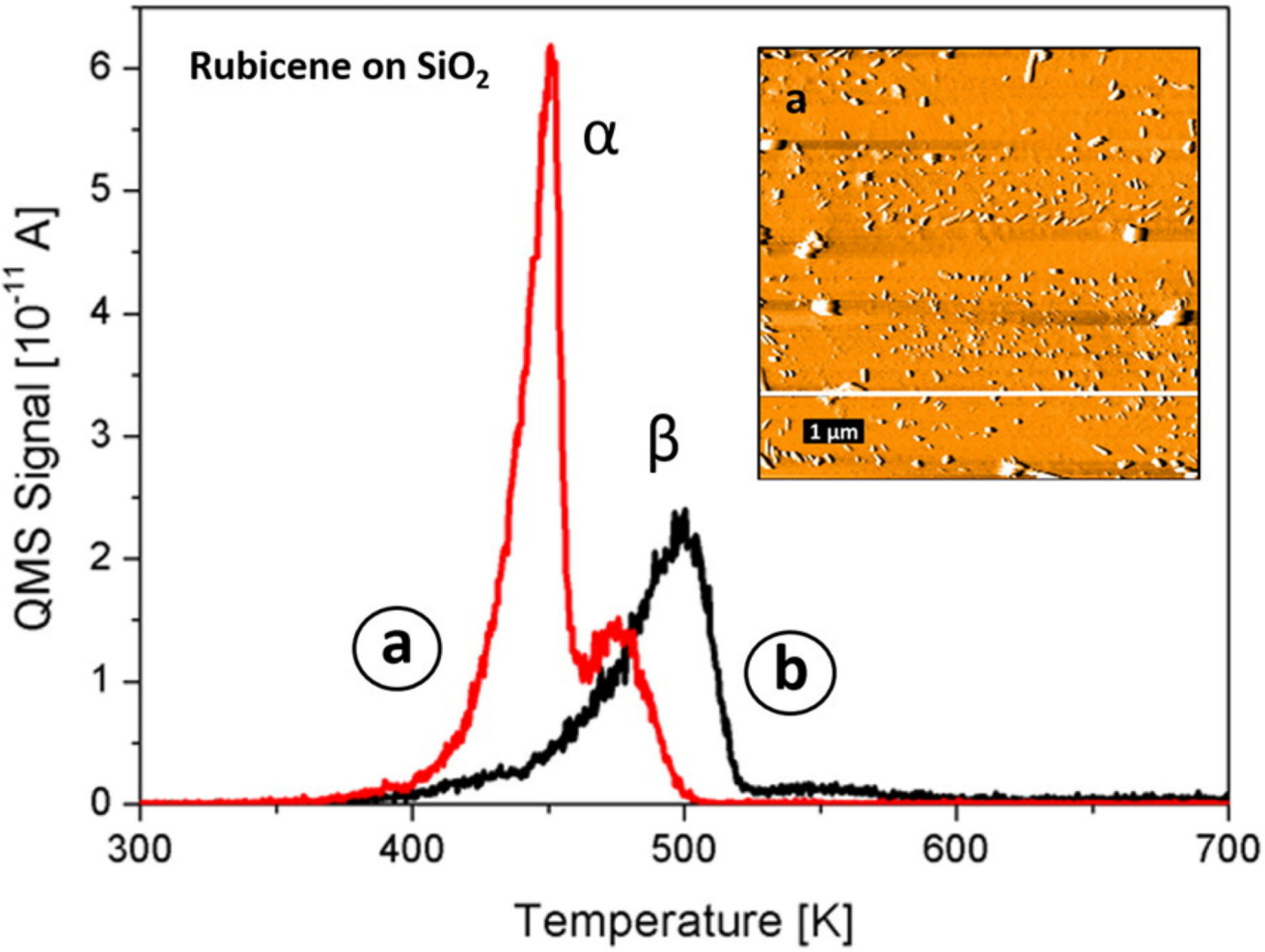

Fig. 19.

Thermal desorption spectra for a 7 Hz rubicene film deposited on C-covered SiO_2 at room temperature directly after deposition (a) and after venting to air and re-evacuation of the vacuum system (b). The cracking mass m = 163 amu was detected. (Reproduced with permission from Ref. [50]).

Europe PMC Funders Author Manuscripts

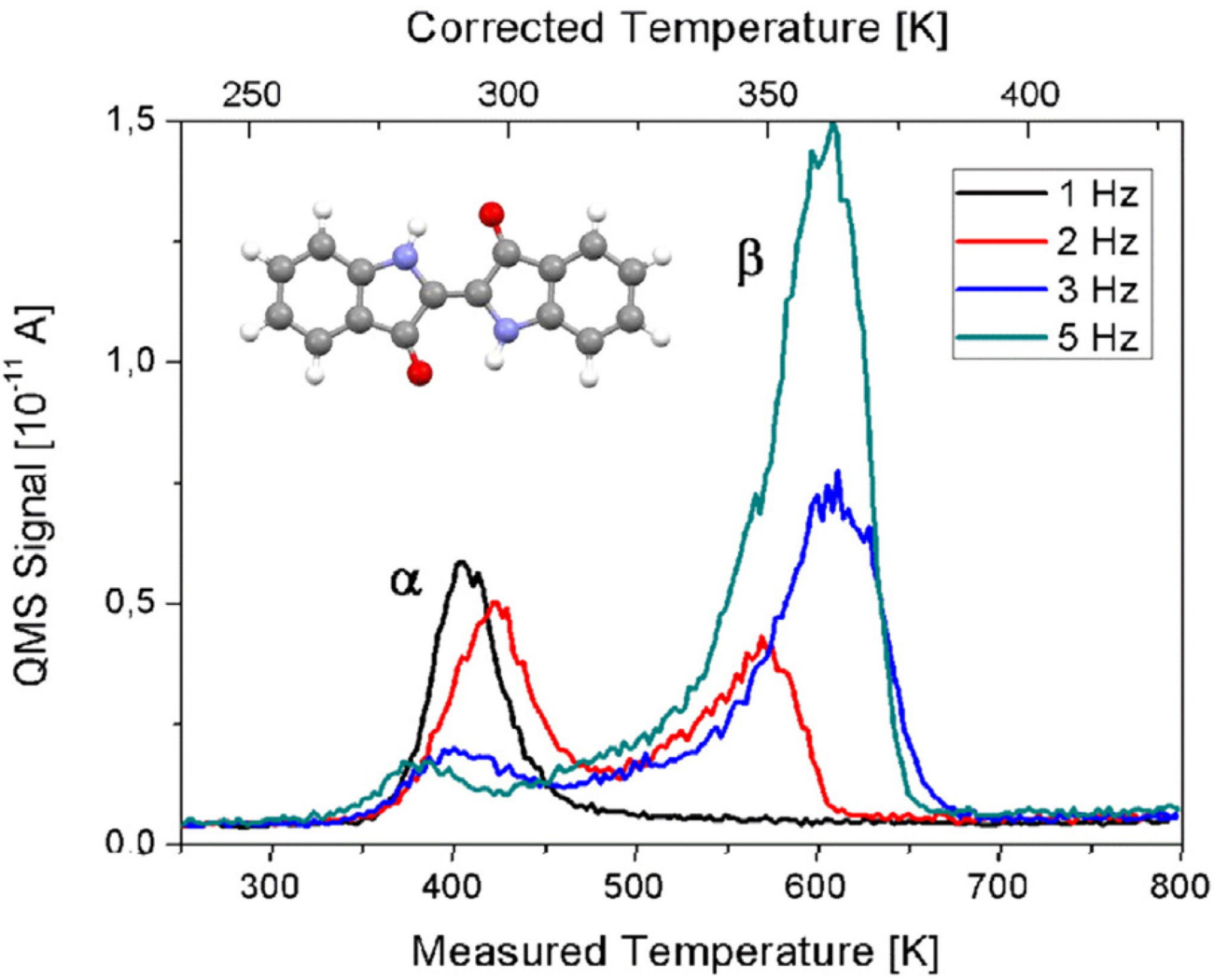

Fig. 20.

Thermal desorption spectra of indigo from carbon-covered silicon dioxide for different exposure. The cracking mass m = 76 amu was detected. 1 Hz equals 0.08 nm indigo. T_{ads} = 220 K, heating rate β = 1 K/s. The chemical structure of indigo is shown in the inset. (Adapted with permission from Ref. [54]).

Europe PMC Funders Author Manuscripts

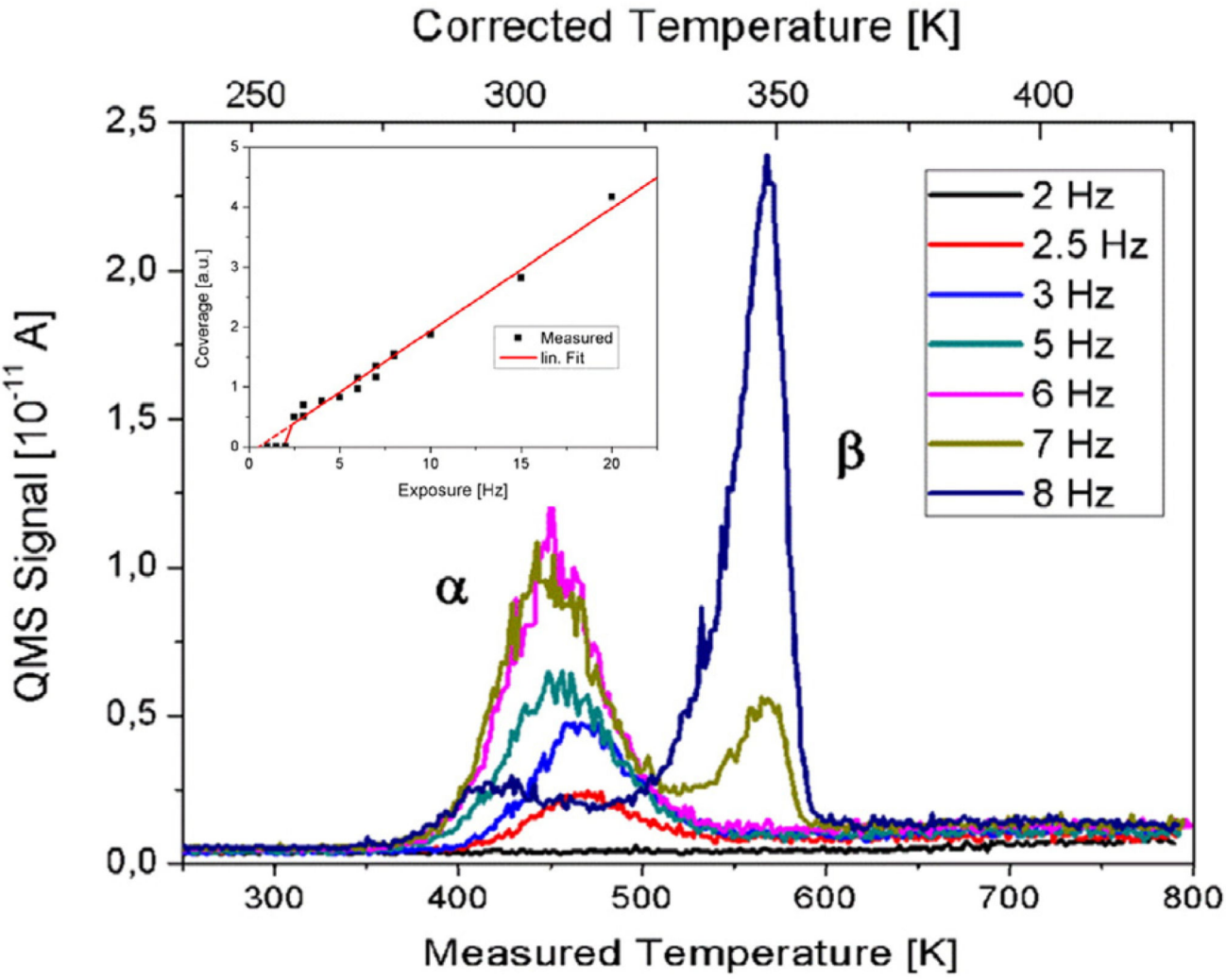

Fig. 21.

Thermal desorption spectra of indigo from sputter-cleaned silicon dioxide for different exposures. The cracking mass m = 76 amu was detected. T_{ads} = 220 K, heating rate β = 1 K/s. The coverage-exposure relationship is shown in the inset. (Adapted with permission from Ref. [54]).

Europe PMC Funders Author Manuscripts

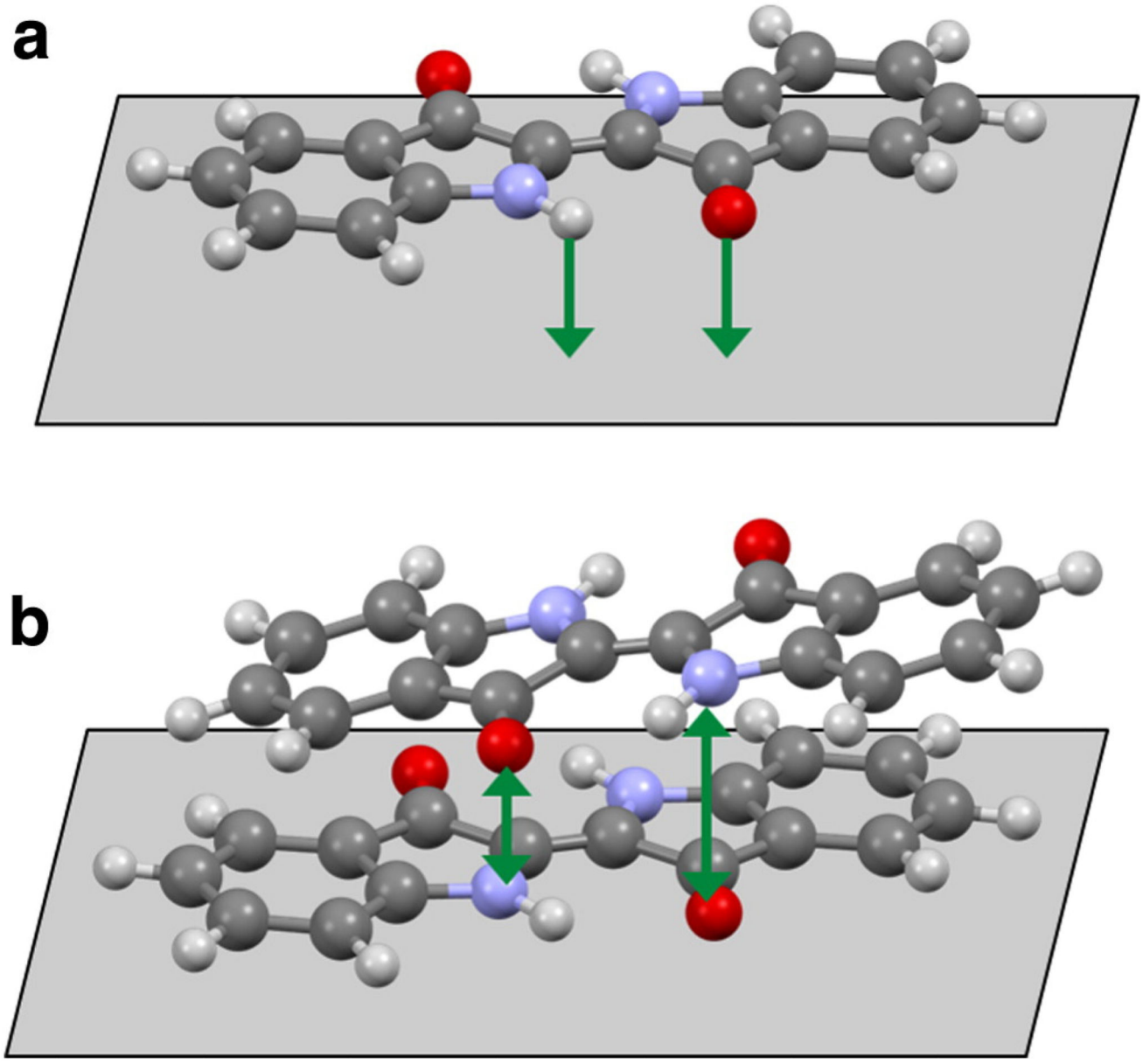

Fig. 22.

(a) Schematics of a single indigo molecule bonded to the silicon dioxide substrate via hydrogen bonds. (b) Suggested dimer formation with intermolecular hydrogen bonds, hereby weakening the bonding to the substrate.

Europe PMC Funders Author Manuscripts

Table 1

Compilation of desorption energies and frequency factors for multilayer desorption of the molecules investigated in this work.

Molecule	Formula	Desorption energy [eV]	Frequency factor [s^{-1}]
Quaterphenyl	$C_{24}H_{18}$	1.5	$2 \cdot 10^{21}$
Sexiphenyl	$C_{36}H_{26}$	2.4	$6 \cdot 10^{25}$
HATCN	$C_{18}N_{12}$	1.8	$1\ 10^{19}$
Rubicene	$C_{26}H_{14}$	1.5	$3 \cdot 10^{18}$
Indigo	$C_{16}H_{10}N_2O_2$	1.7	$1 \cdot 10^{22}$